NTNU – Trondheim
Norwegian University of
Science and Technology

Characterization of Screw Extruded Rapid Solidified AA6061

Thorstein Jacobsen Stedje

Materials Science and Engineering
Submission date: June 2014
Supervisor: Hans Jørgen Roven, IMTE
Co-supervisor: Kristian Grøtta Skorpen, IMT
Oddvin Reiso, IMT

Norwegian University of Science and Technology
Department of Materials Science and Engineering

Declaration

I declare that this master thesis have been done independently and in accordance with the regulations at NTNU.

Trondheim, June 2014

Thorstein Jacobsen Stedje

Acknowledgements

I would like to thank my main supervisor Professor Hans Jørgen Roven for an interesting master thesis and for his dedication to this work. I am also grateful for the help from my co-supervisor, PhD candidate Kristian Grøtta Skorpen for close collaboration and great assistance practically and theoretically. I would also like to thank adjunct Professor Oddvin Reiso for discussions and deep insight in the field.

Further, I would like to thank Trygve Lindahl Schanche, Pål Christian Skaret and Yingda Yu for technical assistance at the micrographic lab, tensile testing and SEM-laboratory.

Abstract

By using rapid solidified aluminium as feedstock and a novel extrusion method, i.e. screw extrusion, it is possible to extrude aluminium continuously. Due to rapid solidification, the base material can have small grain size and super saturated solid solution in the as cast condition. Since consolidation of rapid solidified granulates and particles is an inherent part of the screw extrusion process, conventional consolidation by compaction is redundant. This will give the possibility to extrude a high strength profile with less process steps than used commercially today.

In this study commercially rapid solidified AA6061 is screw extruded at 530°C. The effects of post extrusion heat treatments are documented by microstructure analysis (OM, SEM) and strength (HV1, tensile tests) of the extruded profiles. Six different heat treatment procedures were conducted, e.g. two different T5 and four different T6 conditions.

The results show that this process can give high strength even though the process is not fully optimized. The results from this work indicate that the age hardenability on T5 depends a lot on the quenching rate prior to extrusion. It is found that the solid solution heat treatment (SSHT) and age hardening both have positive and negative effect on microstructure and strength.

Sammendrag

Hurtigstørknet aluminium ekstrudert ved bruk av skrueekstrudering er en kontinuerlig ekstruderingsprosess. Fordelen med hurtigstørknet aluminium er muligheten for å oppnå svært fine korn og et legeringsinnhold i overmettet fast løsning. Ved bruk av skrueekstrudering er ikke lenger sammenpressing av hurtigstørknet granulater til en ekstruderingsbolt før ekstrudering nødvendig. Dermed er det mulig å ekstrudere høystyrke-aluminium ved færre prosesstrinn enn det som benyttes kommersielt i dag.

I denne masteroppgaven er kommersielt hurtigstøknet AA6061 skrueekstrudert ved en dyseteperatur på 530°C. Effekt av varmebehandlingsforløp på de extruderte profilene er dokumenter gjennom mikrostruktur analyse (OM, SEM) og styrke (HV1, strekkprøver). Det er i løpet av studiet sett på seks ulike varmebehandlingsforløp, to ved T5 og fire ved T6.

Resultatene viser at det er mulig å oppnå høy styrke selv om prosessen ikke er optimalisert. Det er funnet ut at grad av bråkjøling etter ekstrudering påvirker utherdingen i stor grad. Det er også vist at innherding og utherding både har positive og negative effekter på styrke og mikrostruktur.

Contents

List of Tables

List of Figures

List of Abbreviations

AAC	Artificial Aging Curves
BS	Backscatter electrons
EDS	Energy Dispersive X-ray Spectroscopy
OM	Optical Microscope
RS	Rapid Solidified/Solidification
RSA	Rapid Solidified Aluminium
RSA6061	Extruded profile of RSP6061
RSP	Rapid Solidification Process
RSP6061	Rapid Solidified ribbons/granules from RSP-Technology
SD	Standard Deviation
SE	Secondary Electrons
SEM	Scanning Electron Microscope
SSHT	Solid Solution Heat Treatment
UTS	Ultimate Tensile Strength
YS	Yield Strength

1. Introduction

The use of the screw extruder to extrude rapid solidified aluminium is not a commercial process today. Screw extrusion is a novel continuous extrusion method that makes it possible to extrude melt spun granules and aluminium granulates. By using the screw extruder there is no need for a consolidation step prior extrusion and the use of rapid solidified aluminium do not need any heat treatment step before extrusion to get good extrudeability and good strength. By using rapid solidified aluminium and screw extrusion there is possible to make a high strength material with less energy input, than in commercial processes used on rapid solidified aluminium today. There have been several master theses and a PhD candidate on screw extrusion of aluminium before [1-6], but this will be the first published work with rapid solidified aluminium.

In this master thesis there are used rapid solidified AA6061, that were melt spun by RSP-Technology[7]. The material was screw extruded in house at NTNU, with process parameters based on PhD Candidate K. Skropen experience. The effect of age hardening of “as extruded” profiles and the effect of solid solution heat treatment temperatures are studied. The microstructure and strength have been analysed in six different heat treatments, two T5 and four T6. The positive and negative effects are discussed and further work is proposed.

2. Theory

2.1. Material

The 6000 alloy series is a group of heat treatable wrought alloys, with the main alloying elements magnesium (Mg) and silicon (Si). These alloys are highly used in extruded profiles due to good extrusion and corrosion resistance. This alloying system can also have other elements such as manganese (Mn) and chromium (Cr), and both work as a grain refiner and formation of dispersoids. To get even higher strength, these alloys can be alloyed with a small amount of copper (Cu). The typical composition of the 6000 series is given in Table 1[8].

Table 1: Typical main element composition range of the 6000 series [wt%].

	Si	Mg
6xxx	0.5-1.3	0.4-1.4

In Figure 1 and Figure 2 the Al-Mg_2Si phase diagram and the respective solidus temperatures for the Al-Mg-Si system are illustrated. The equilibrium temperature for Al-Mg_2Si system is 595°C, and the solibility of Mg_2Si at this temperature are 1.85 wt%. This is the maximum solibility of Mg_2Si, and with decreasing temperature, the solibility deacrese to ~0.3wt%. The eutectic point is at ~16wt% as seen in Figure 1.

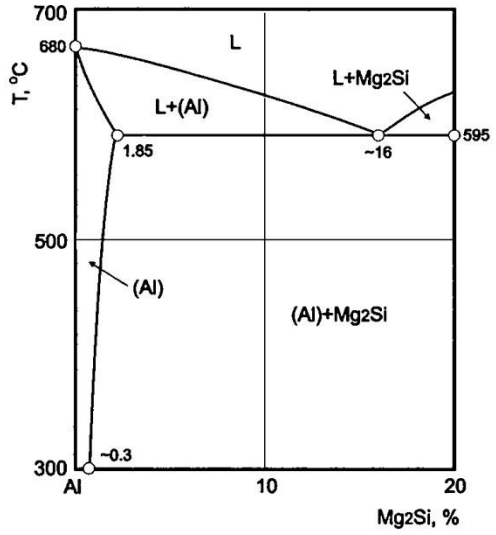

Figure 1: Al-Mg_2Si phase diagram in [wt%] [9].

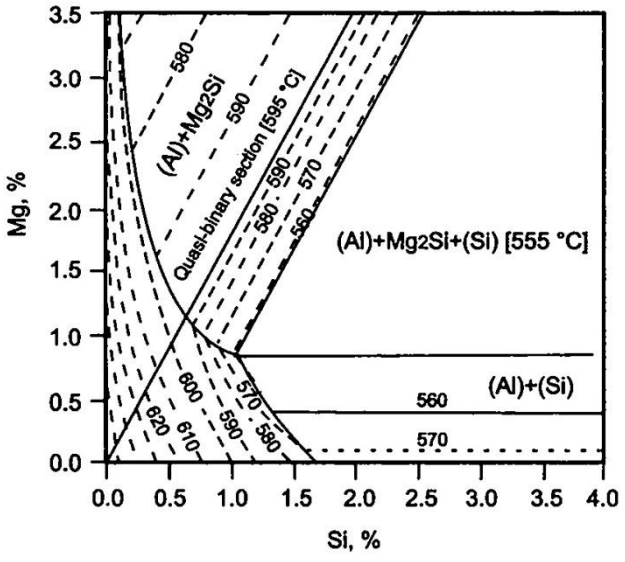

Figure 2: Solidus section of the Al-Mg-Si system with Mg and Si in [wt%] on the respective axis[9].

The β-phase (Mg_2Si) is the equilibrium phase of Al-Mg-Si alloys. This phase can either be nucleated during solidification, or by precipitating in the solid aluminium

phase. The growth mechanism of Mg_2Si is described by Li, C.[10], where the Mg_2Si prefer to grow in 100 direction, followed by 111. This gives polygonal particles with straight edges, which occurs during solidification and precipitation[11].

2.2. Screw extrusion

The extrusion process in this study is screw extrusion. This is a method develop in cooperation between NTNU and Hydro Aluminium R&D[12]. The main difference from conventional billet extrusion is that screw extrusion is continuous and the feeding material is granulates or cut ribbons, instead of billets. To the best of the authors knowledge, the screw extruder for metals at NTNU is the only in the world.

The extruder is schematically drawn in Figure 3. The purpose of the screw extruder is to mechanically deform and compact small metal granules into a solid profile. The principle is the same with granules and rapid solidified ribbons. First the material is placed in a feeder that gives a steady feeding rate into the feeding hole. Then the material is pushed forward by the flange in the screw. The material compacts due to pressure at the end of the screw and container walls. When the pressure is built up to a certain point extrusion of profiles begins[5]. When extrusion has started, the heat generated from friction and deformation is significant. The temperature in the extruder is controlled by induction of the die and air-cooling in the back chamber. In the present set-up there are eight thermo elements to monitor the temperature, from the die opening back to the feeding hole. Various die opening geometries can be utilized, such as found, flat or hollow, e.g. for rod-, narrow extrusion plates and pipes respectively. The smaller the cross-section area of the die opening, the larger is the extrusion ratio.

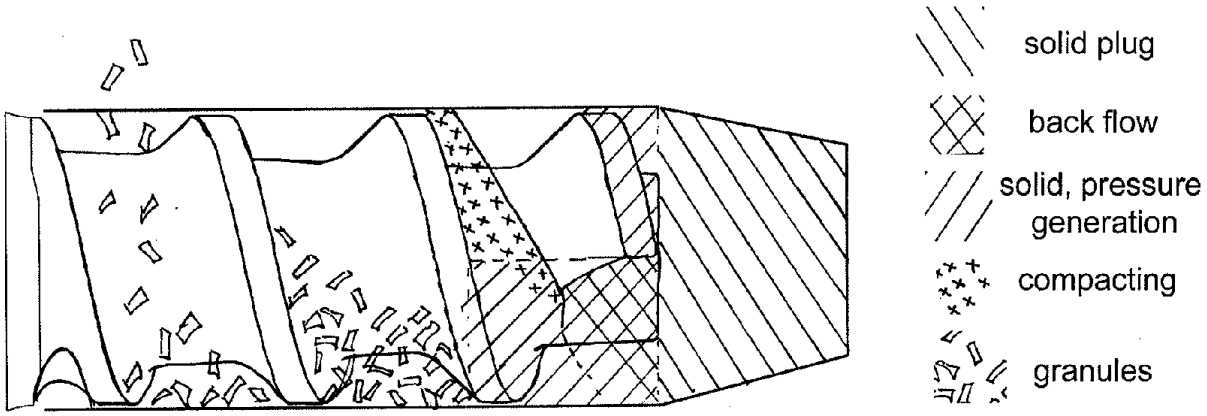

Figure 3: Schematic drawing of the in-house developed screw extruder at NTNU[12].

2.3. Heat treatment

The typical thermal history for an extruded and heat treated aluminium alloy can be seen in Figure 4. Starting with DC-casting, then homogenisation and extrusion and finishing with artificial aging. Normally a solid solution heat treatment is done

between extrusion and artificial aging. The processes that are being described in this chapter are SSHT, artificial aging and natural aging. It is normal to describe the thermal state of the material with abbreviations and the most important in this case is seen in Table 2.

Table 2: Standard heat treatment codes for aluminium alloys[13].

Abbreviation	Description
F	As fabricated/extruded (no heat treatment after extrusion)
W	Solid solution heat treated and quenched
T5	Extruded followed by artificial aging to peak strength
T6	SSHT and artificial aged to peak strength

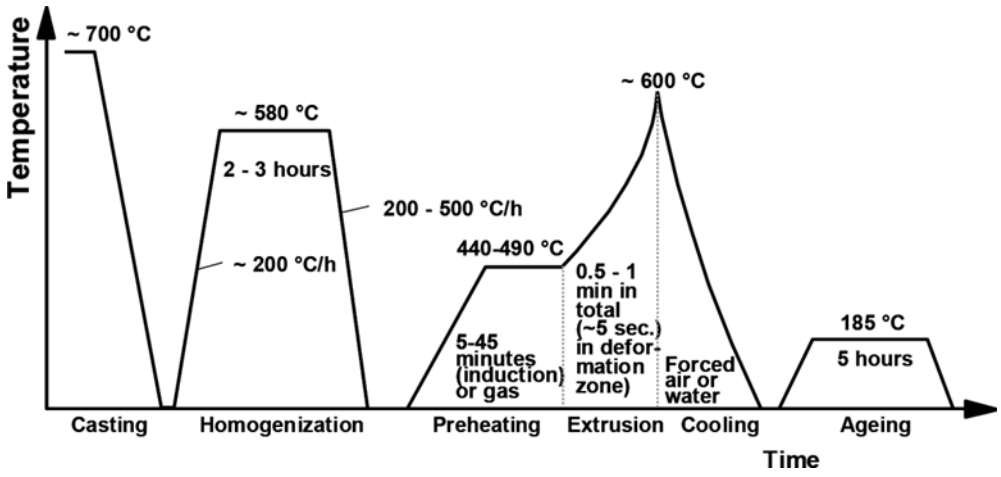

Figure 4: Typical commercial thermal history of extruded profiles[14].

2.3.1. Solid solution heat treatment

The aim of solid solution heat treatment of an extruded profile is to get the main alloying elements in solid solution. This is done by heating the profile close to the eutectic temperature and holds it for some time, and then cooling the profile in a rapid manner. The amount of elements in solid solution is controlled by the chemical composition, solvus line and the cooling rate. By quenching the concentration of elements should be roughly the same as at the SSHT temperature, i.e. super saturated solid solution. As seen in Figure 1 the maximum solubility of Mg_2Si is 1.85wt% at 595°C and less than 0.3wt% at room temperature.

A secondary effect of solid solution heat treatment is the change in electric conductivity. With an increasing amount of alloying element in solid solution, the electric conductivity is decreasing[15].

2.3.2. Artificial aging

The main goal of artificial aging is to precipitate particles that give a strength contribution. This is done by heat treatment of the material for a specific time at a

specific temperature. The time and temperature depend on the alloy chemistry and microstructure. The precipitation sequence for AA6000 alloys is [8]:

$$SSSS \rightarrow GP1 \rightarrow \beta'' \rightarrow \beta' \rightarrow \beta(Mg_2Si)$$

Where SSSS is super saturated solid solution, GP1 is small needles of $AlMg_4Si_6$ or plates of SiMg, β'' is needles of $Mg_5Si_{6,}$. β'is a more complex structure and not well defined. There are up to five different precipitates that are in the latter group [8, 16]. The precipitation sequence can also be imagined from Figure 5, i.e. showing the Al-Mg_2Si phase diagram with the respective solvus lines for the various precipitation phase-zones. The equilibrium phase is Mg_2Si. Moreover, the strengthening contribution from precipitates is explained in more detail in section 2.7.

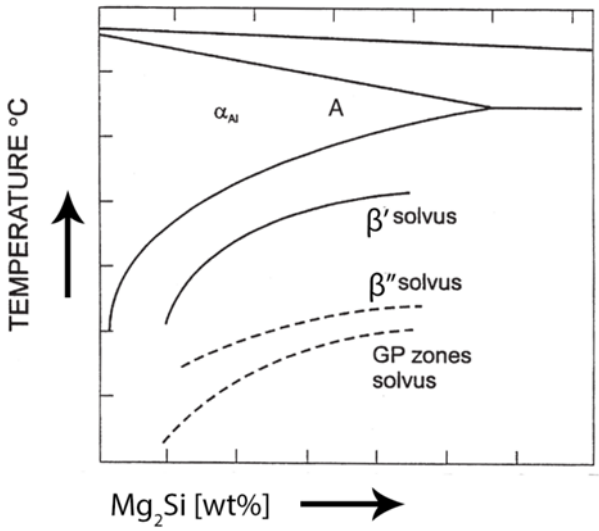

Figure 5: Sketch of solvus lines for metastable precipitation zones (based on fig 2.1 [17]).

Precipitation is dependent on aging temperature and time. For a low aging temperature, the time needed to achieve maximum strength is longer compared to aging at high temperature. It is common to use a constant aging temperature and then look at the time for maximum strength. The maximum strength for Al-Mg-Si alloys appears when the β'' is the dominating precipitate. If the material is aged for too long, β'' will transform to β'and even further Mg_2Si (β-phase). This is further described in section 2.7.

The precipitation can be enhanced by second particles. There has been observed by Dons et al.[18] and described by O. Reiso[14] that coarse β' and β will nucleate at Mn and Cr dispersoids with a higher rate than without the stated elements. Chrome are observed to have the biggest impact on the formation of β' and β.

2.4. Natural aging

The principle for natural aging is the same as for artificial aging. The main difference is that aging is performed at room temperatures and the time for maximum strength to occur is significantly larger. The transformation from solid solution to GP- zones is controlled by diffusion which is explained in more detail in section 2.6. The alloy 6061 will be close to maximum strength during natural aging, after aging in 10^5 hours. There is an increase in strength (25%) after about 10 to 100 hours at room temperature, but after that the strengthening stagnates [13].

2.5. Recovery, recrystallization and grain growth

The three phenomena recovery, recrystallization and grain growth are close related processes. These processes will lower the internal stored formation energy for the material am hence reduce the effect of cold/hot work on the material. Grains with the same crystallographic structure (bcc, fcc etc.) will have different crystallographic orientations. The miss-orientation between grains at the grain boundary is an important factor. There are two main expressions for this, low and high angle boundaries[19]. Recovery and recrystallization are also defined as discontinues and continues, where continues means that the microstructure evolves with no clear distinction two between the phenomena. While discontinues describe processes happening heterogeneously through the material[19]. In deformation processes like extrusion and screw extrusion discontinues recovery and recrystallization can be assumed. The main annealing stages are shown in Figure 6 and described below.

Recovery is the first step of the process. This happens at low heat input to the material, but at elevated temperature. During recovery the dislocation density will be lowered, and subgrains will grow. The boundaries between subgrains will be gradually dislocation free. This will reduce the ultimate tensile strength (UTS) and yield strength (YS) of the material, but also increase the elongation at fracture.

Recrystallization will change the appearance of the grain structure. New grains will nucleate on strain fields, old grains boundaries, subgrain boundaries or particles. There is normally a mix of sites where nucleation starts. For extrusion the phenomenon of high angle boundaries (HAGBs) is a likely assumption. During screw extrusion of rapid solidified many small RS-ribbons are forced together and high angle boundaries are formed. With HAGBs as nucleation sites recrystallization is normally continues with random nucleation and growth of grains. High angled misorientated subgrains have high probability to start recrystallization. However, low angle grains are more resilient to recrystallization[20].

Finally recrystallization is followed by grain growth. Grain growth is dependent on neighbouring subgrains and grains. If the material have a strong texture (low misorientation between neighbour grain boundaries), grain growth can happen, but the driving force is low [20]. When grain growth happens at low angle grains, the

resulting grains are abnormally big [21]. This is often seen at the surface of extruded profiles, i.e. due to high strains and strong texture. Second phase particles can supress grain growth, by being a physical barrier for grain boundaries and hence an energy barrier.

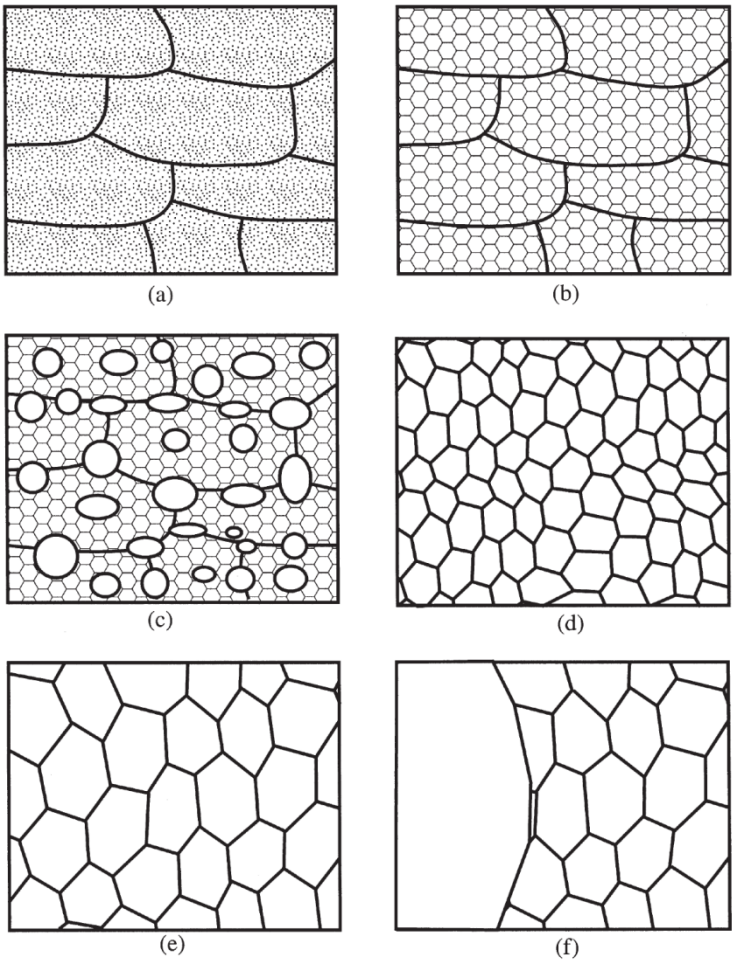

Figure 6: Schematic diagram of annealing stages; (a) deformed state, (b) recovery, (c) partially recrystallized, (d) fully recrystallized, (e) grain growth and (f) abnormal grain growth[20].

2.6. Diffusion

The diffusion of atoms in alloys is dependent on Gibbs free energy. The atoms will diffuse to the area that gives lowest possible Gibbs free energy for the system under consideration. There are two types of diffusion in metals; interstitial and substitutional. Interstitial means that atoms are in between the hosting crystallographic lattice. In other words the interstitial atoms are much smaller than the atoms in the lattice, and diffusion will occur between the matrix atoms. For substitutional diffusion, the atoms constituting the lattice will diffuse from one place to another through the matter. For this to be possible, lattice atoms and vacancies change position, and the atoms need have an energy larger than the activation energy for vacancy diffusion. The main parameter for diffusion is temperature. The

temperature affect the vibration/energy of the atoms by 3kT, were k is the Boizman constant and T the temperature in [K]. This means that, at higher temperatures, the possibility for diffusion is higher and diffusion rates are more rapid[22].

However diffusion does not occur only in the lattice, but also along grain boundaries, free surfaces and dislocations. These are considered high diffusive paths. The diffusion along grain boundaries are faster than in the lattice, but due to low thickness (δ) of the grain boundaries, diffusion has to be scaled by $\frac{\delta}{d}$, where d is the grain size. In Figure 7 this principle is shown and explains how temperature affects the relation between grain boundary and lattice diffusion. Lattice diffusion will dominate when the temperature is over a certain point, which is 0.75-0.80 T_m, where T_m is the melting temperature. This can be seen from Figure 7, by following D_{app}, which represents the dominant diffusion mechanism[22].

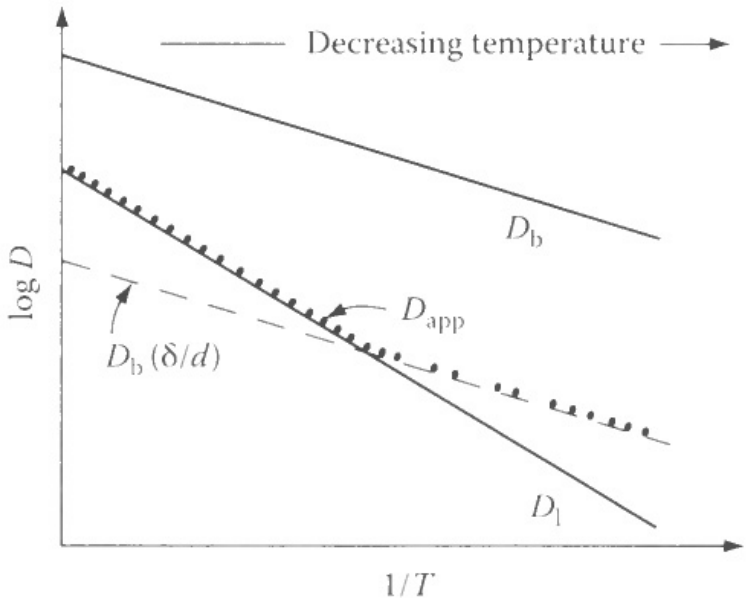

Figure 7: Diffusion coefficient D, with it dependency to temperature [22].

Diffusion along dislocations is negligible at higher temperatures, but at lower temperatures dislocation diffusion is dominating. This is due to a lower activation energy [22].

2.7. Strengthening mechanisms

There are several different strengthening mechanisms that are important for aluminium alloys, and the most important in this case is grain boundary and secondary phase particle strengthening.

2.7.1. Solid solution strengthening

There are two types of types of solid solution, interstitial solid solution and substitutional solid solution. Interstitial solid solution, the solute atoms are much

smaller than the solvent atoms. Then the solute atoms will be in between the solute atoms lattice. Substitutional solid solution, the solute atoms take place in the solvents lattice. Alloying elements in solid solution is favourable if the lattice parameter difference for the solvent and solute is less than 15%, and therefor favourable for solid solution strengthening.

There are five main strengthening effects from solid solution, elastic-, modulus-, stacking fault-, electrical-, short-range order- and long-range order interaction. Where these five can be divided into short-range order (stacking fault and short-range) and long-range order (elastic, modulus and long range). Short-range only give strength contribution on low temperatures, while long-range order up to 60% of the melting temperature. An increasing amount of alloying element inn solid solution will increase the yield strength and tensile strength[15, 23].

2.7.2. Grain boundary strengthening

Grain boundaries have big effect on the yield stress and strain hardening. The strain hardening rate for a polycrystalline FCC material is 9.5 times higher than in a single crystal[23]. The most important factor for grain boundary strengthening is the Hall-Petch relation[23]:

$$\sigma_0 = \sigma_i + kD^{-1/2} \qquad (1.)$$

Where σ_0 is the yield stress [MPa], σ_i the lattice friction stress for a gliding dislocation, k the locking parameter (relative stress intensity contribution of the grain boundaries) [MPa*$m^{0.5}$] and D the grain diameter [m]. The equation shows that smaller grains give higher yield strength than big grains. The $\frac{1}{\sqrt{x}}$ relation for D, give an increase in yield stress with diminishing grain diameter. The model used for describing Hall-Petch equation is that grain boundaries work as a barrier for dislocations, so the dislocations will pile up at the boundary. For a given dislocation density, small grains will have less dislocations piled up than big grains. From shear stress relations one can derive that small grains will have less piled up stress and the probability for crack propagation is therefore smaller.

2.7.3. Particle strengthening

The effect of second phase particles in a matrix of ductile material is called precipitation hardening. The particles are normally formed in a sequential manner as described in section 2.3.1. The particles that are precipitated can either be coherent with the matrix or not, and the coherent phases give a local strain field that increase the hardness. The coherent particles grow in the same planes as the matrix, but the c-axis is smaller, hence there will be a strain field around the particle (see Figure 8)[8]. The finer distribution of particles, the higher is the strength, i.e. due to homogeneous strain fields in the material.

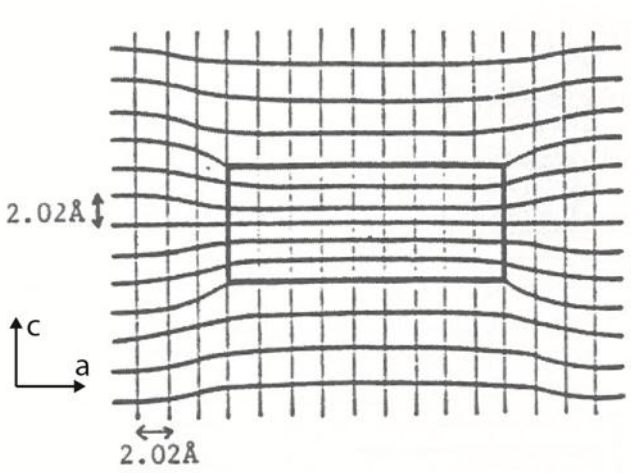

Figure 8: Schematic drawing of a coherent particle and the associated displacement of the matrix lattice[8].

The β′′ is coherent with the matrix and therefore have the largest hardening effect, while GP1 and β′ are partly coherent. The β is incoherent. As seen in Figure 9 the particle size get bigger throughout the aging process.

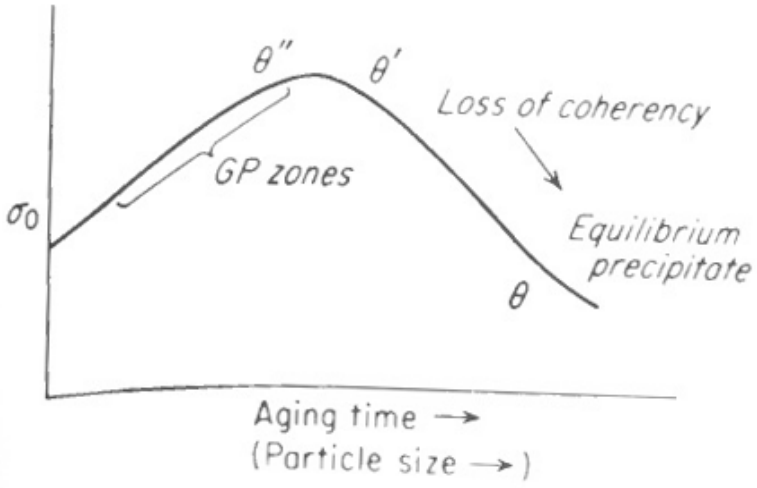

Figure 9: Precipitation sequence and yield strength development upon artificial aging, θ (Al_2Cu) is here the equivalent to β in AlMgSi alloys[23].

Particles give a strengthening effect because dislocations have to move through or around the particles. If the particles are small and soft i.e. coherent, the dislocations have to cut through the particles, as shown in Figure 10. The energy needed for cutting the particle is greater than for moving through the matrix and therefor the amount of energy needed for yielding gets higher. If the particles are stronger (incoherent) and further away from each other, the dislocations can move around the particle and normally make a dislocation loop around the particle (see Figure 11). As a consequence the strain field around the particle will increase and the material strain-hardens, due to a higher dislocation density[23]. In other words,

incoherent particles are assumed as strong, while the coherent are weaker and therefore cut by gliding dislocation.

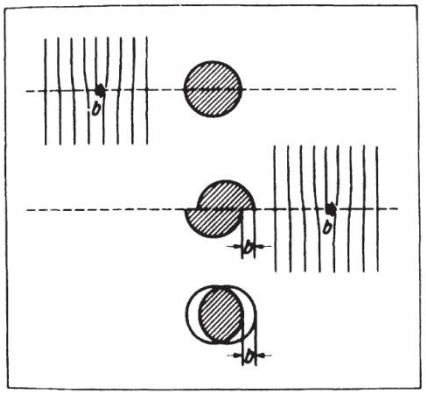

Figure 10: Cutting of particles by gliding dislocation[17].

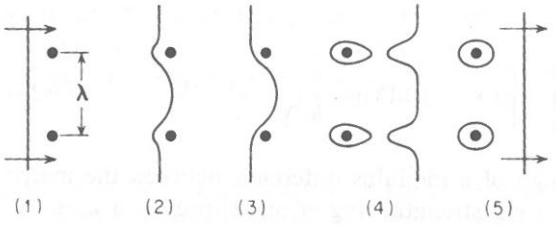

Figure 11: Dislocation movement and interaction with strong (incoherent) particles[23].

2.8. Fractography

The different fracture mechanisms in metals can be defined in different was, but the most common used is; brittle fracture, ductile fracture and fatigue fracture.

Brittle fracture is described that the elongation is minimal and the fracture surface cuts through grains (transcrystalline) on crystallographic planes or on the grain boundary (inter crystalline) without plastic deformation.

Ductile fracture there is local deformation in the material. The deformed material will get a “dimple structure”, this form due to plastic deformation in the material. The dimples will often propagate due to particles in the material, therefor small particles can be seen in the centre of a dimple. In Figure 12 a schematic drawing of dimple propagation in a ductile fracture, in a) tensile load, b) shear stress and c) tearing[24].

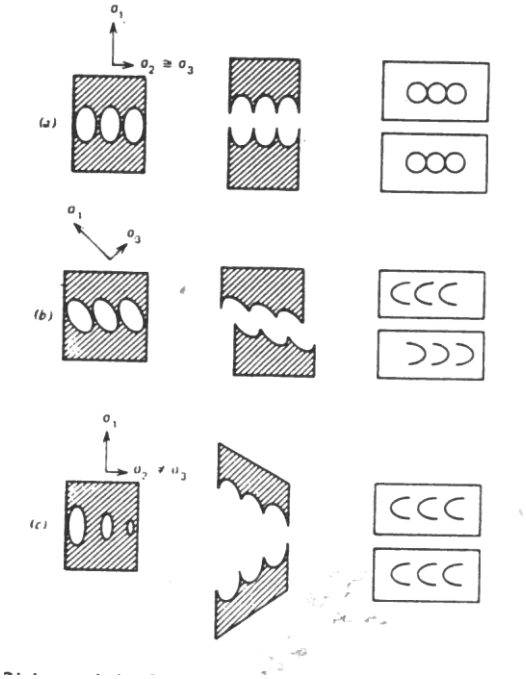

Figure 12: Schematic drawing of ductile fracture[24].

2.9. Vickers Hardness

The Vickers method measures the hardness by pressing a diamond pyramid indenter into the material. The indenter is pressing with a given load (P) and the two diagonals of the diamond shaped indent are measured. By using equation 2, where L is the mean of the diagonals in millimetre, P load in kilograms and the Vickers hardness (HV) can be found [23]:

$$HV = \frac{1.853P}{L^2} \qquad (2.)$$

2.10. Scanning electron microspy

The scanning electron microscope (SEM) is a microscope that uses an electron beam which is stationary or swipes the surface of the sample. The sample has to be electrically conductive, either by itself or by a layer of conductive material on the sample. When the electron beam hits the surface several signals will be reflected, and the most important in this case are backscatter electrons and secondary electrons. Secondary electrons are used for topography and typical fractography images. Backscatter electrons are used for z-contrast which will give a contrast from the different chemical elements in the sample. A higher atom number (Z) will return a larger amount of electrons than a lower atom number. From this, a high atom number particle will be brighter than the surrounding matrix having a lower atom number. The emission depth (R_{bs}) of electrons is illustrated in Figure 13, were a high acceleration voltage will increase the emission depth as well as low atomic numbers will increase their emission depth.

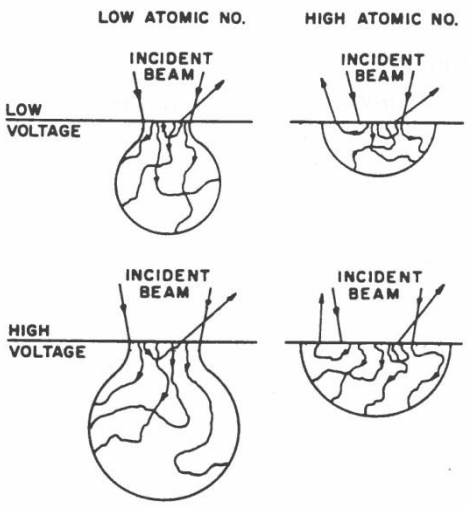

Figure 13: Emission depth of backscatter electrons[24].

The emission depth depends on the different parameters shown in equation 3[24].

$$R_{bs} = \frac{8.3 * 10^{-3} * A * E_0^{1,67}}{Z^{0,889}\rho} \qquad (3.)$$

Where E_0 is the electron beam energy [keV], A is atom weight [g/mol], ρ is density [g/cm^3] and Z is the atom number.

In order to determine the different elements in a sample, energy dispersive spectrum (EDS) is normally used. The EDS detector detects x-rays that are emitted from the sample. Different elements have different characteristic wavelengths that are emitted, either from the K-shell or L-shell in the atom. The mission depth of x-rays for aluminium can be found in Figure 14.

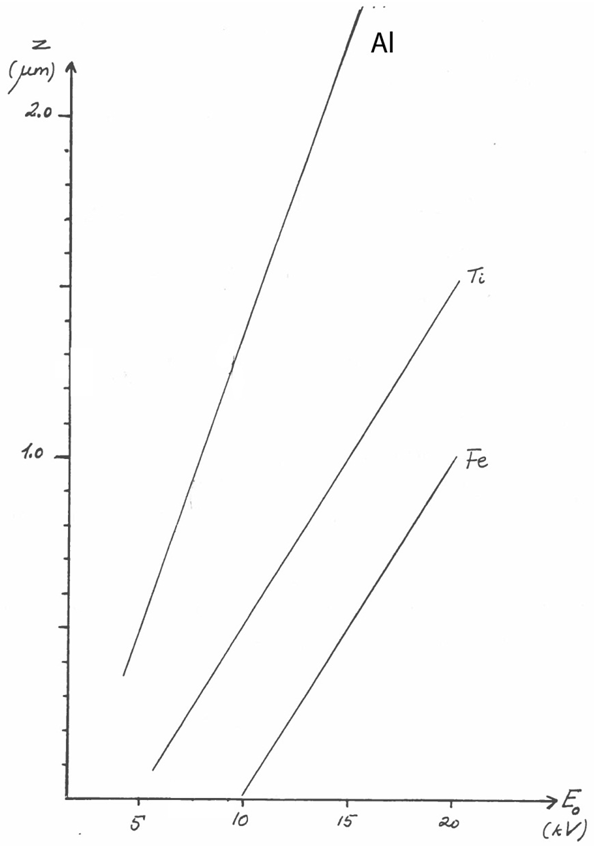

Figure 14: Emission depth as function of the electron beam energy for characteristic K-shell x-rays in aluminium, titanium and iron[24].

3. Experimental

An overview of the experimental procedures is shown by the three flow charts in Figure 15, Figure 18 and Figure 19. They describe three different stages in the study. The first, seen in Figure 15 describes the investigations on rapid solidified granulates (RSP6061), preparation before extruding and extrusion. The second stage, seen in Figure 18 shows the first analysis procedures for the extruded profiles (RSA6061). After the results were obtained in the second stage, a third stage of investigations were performed, see Figure 19. More detail of the various process steps are described later in this chapter. Please note that rapid solidified granules are named RSP6061, while extruded profile are named RSA6061.

The hexagons in these figures represent investigations on feedstock and profiles, while the squares are processing or analysis steps. The red hexagon locates the extruded profiles, which are used in stage two and three.

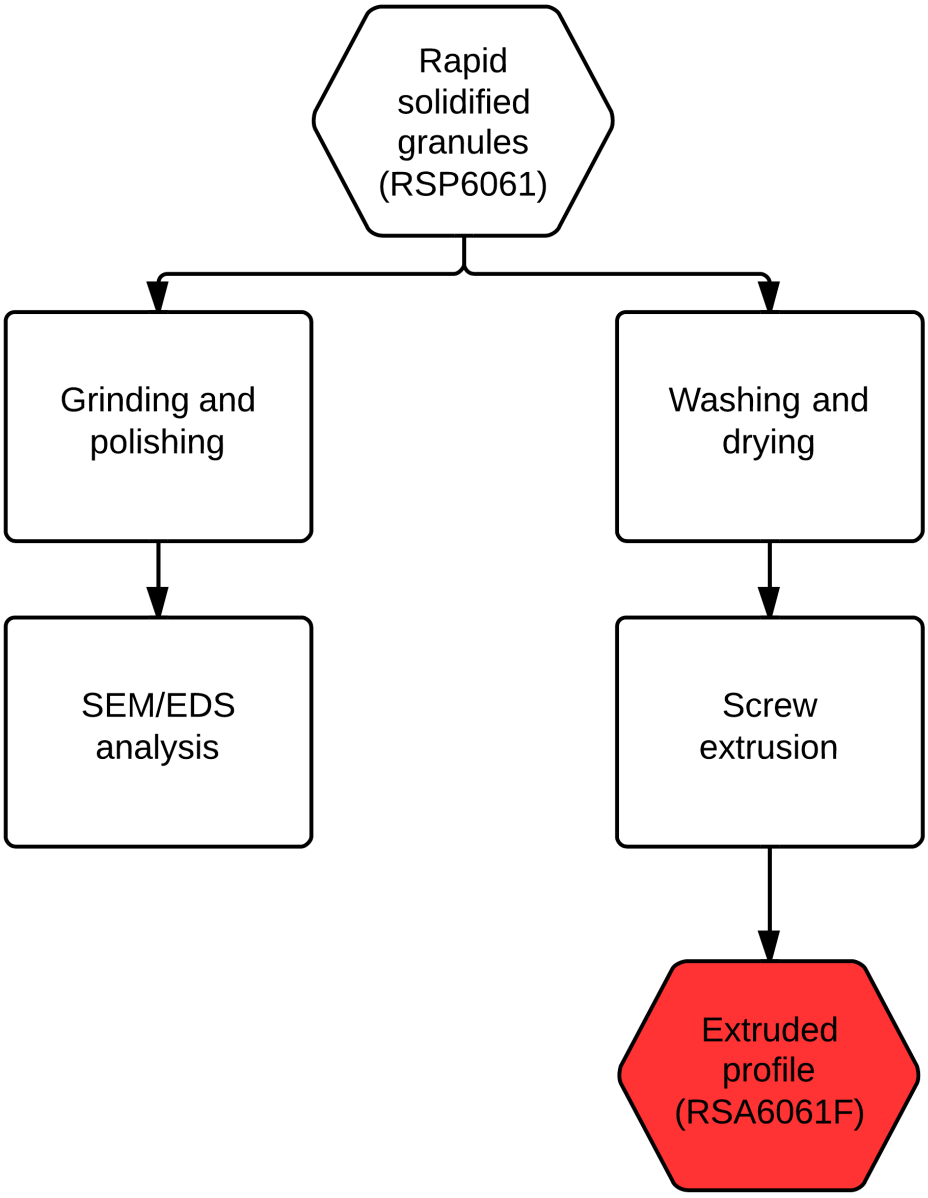

Figure 15: Flow chart of analyses and processing of AA6061 rapid solidified ribbons cut into granulates, supplied by the company RSP-Technology in the Netherlands.

3.1. Rapid solidified ribbons (RSP6061)

The material used in this study is RSP6061 (Figure 16), which is an AA6061 alloy, rapid solidified at "RSP-Technology"[25]. The ribbons were cut into finer fragments and by this some mechanical deformation was introduced. The expected and measured (exact) compositions are shown in Table 3. The exact composition was obtained at Hydro Sunndal and an average of five samples was used for this purpose.

Figure 16: Representative collection of the granulates (cut from ribbons) obtained from RSP-Technology, Alloy RSP6061.

Table 3: Composition of RSP6061 [wt%].

	Si	Fe	Cu	Mn	Mg	Zn	Ti	Cr	Al
RSP6061 Expected[26]	0.6	*	0.3	*	1	*	*	*	Balance
RSP6061 Exact	0.71	0.12	0.28	0.12	1.05	0.005	0.09	0.21	Balance

3.1.1. Material properties

The expected properties in temper T6 forRSP6061 profiles produced by RSP-technology are shown in Table 4. The procedure for obtaining T6 temper at RSP-Technology was unfortunately unavailable.

Table 4: Expected material properties for RSP6061 (T6) as given on RSP-Technology data sheet[26].

	Yield strength [MPa]	UTS [MPa]	Elongation [%]	Hardness [HB]
RSP6061	300	330	14	110

3.2. SEM analysis of RSP6061granulates

A SEM analysis of the RSP6061ribbons was performed. The granules were first grinded with 2000 SiC paper followed by polishing with 3µm and 1µm diamond spray, and a lubricant without water (ethanol based). This was done by flattening

the granule, taping it to a plexi glas piece by a double sided tape and then grinding and polishing, by hand.

Before the prepared granules were taken into the SEM, the samples were washed in acetone and then dried in air. The specimens were taped to the SEM sample holder with a carbon tape. The analysis was performed with secondary electrons for topography and backscatter electrons for z-contrast issues. EDS was used for element analysis when needed.

3.3. Screw extrusion

The extrusion was done by screw extrusion. Before extrusion, the granules were washed in acetone and water followed by drying in air at room temperature. This procedure is based on the previous studies of Audun Bilsbak [1].

The extruder was then preheated to the desired temperature, and the die temperature during extrusion was as close to 530°C as possible. This temperature was more or less (±10°C) stable during the extrusion, as seen in Figure 17. Further, the rotation speed of the screw was increased from 8 RPM to 10 RPM during the extrusion. For the feeding rate, this was controlled to get a highest possible input of material without pile up of material to occur. As a consequence, the feeding rate was not constant. The profile was cut with a bolt cutter during the extrusion in lengths of 30 to 40 cm, 10cm from the die opening. After the profiles were cut, they were quenched in a water bath at a temperature less than 20°C. Hence the front part of the profile (RSA6061F Front) did get a longer chilltime in air than the back part of the profile (RSA6061F Back), before quenching.

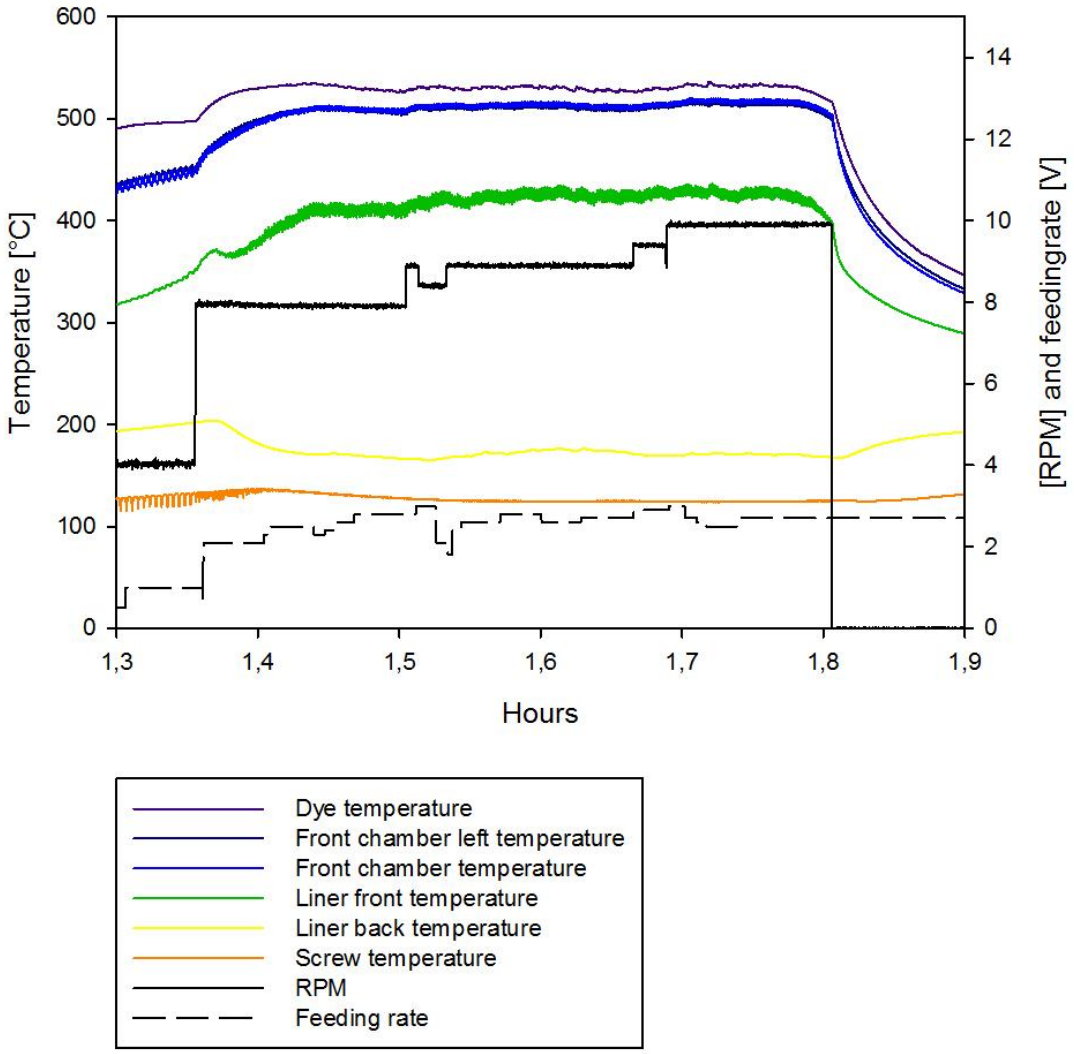

Figure 17: An overview of the screw extrusion parameters measured by the instrumental set-up. Note that feeding rate is described of the input feeding rate voltage, not exact feeding rate.

To get an estimate of the extrusion speed the time was taken for six profile pieces. The time was taken with a stopwatch for every cut and the corresponding profile lengths were measured with a ruler.

3.4. Process steps preformed on screw extruded profiles

Figure 18 and Figure 19 illustrate flow charts for the process steps preformed on the screw extruded profiles. It should be noted that all material used in these steps were from the same extrusion. In the investigations shown in Figure 18, the solid solution heat treatment issues here were to investigate the effects of "front" and "back positions of the cut profiles on hardness and microstructure and compare the T6 and T5 tempers as to mechanical properties and microstructure for the T5 temper.

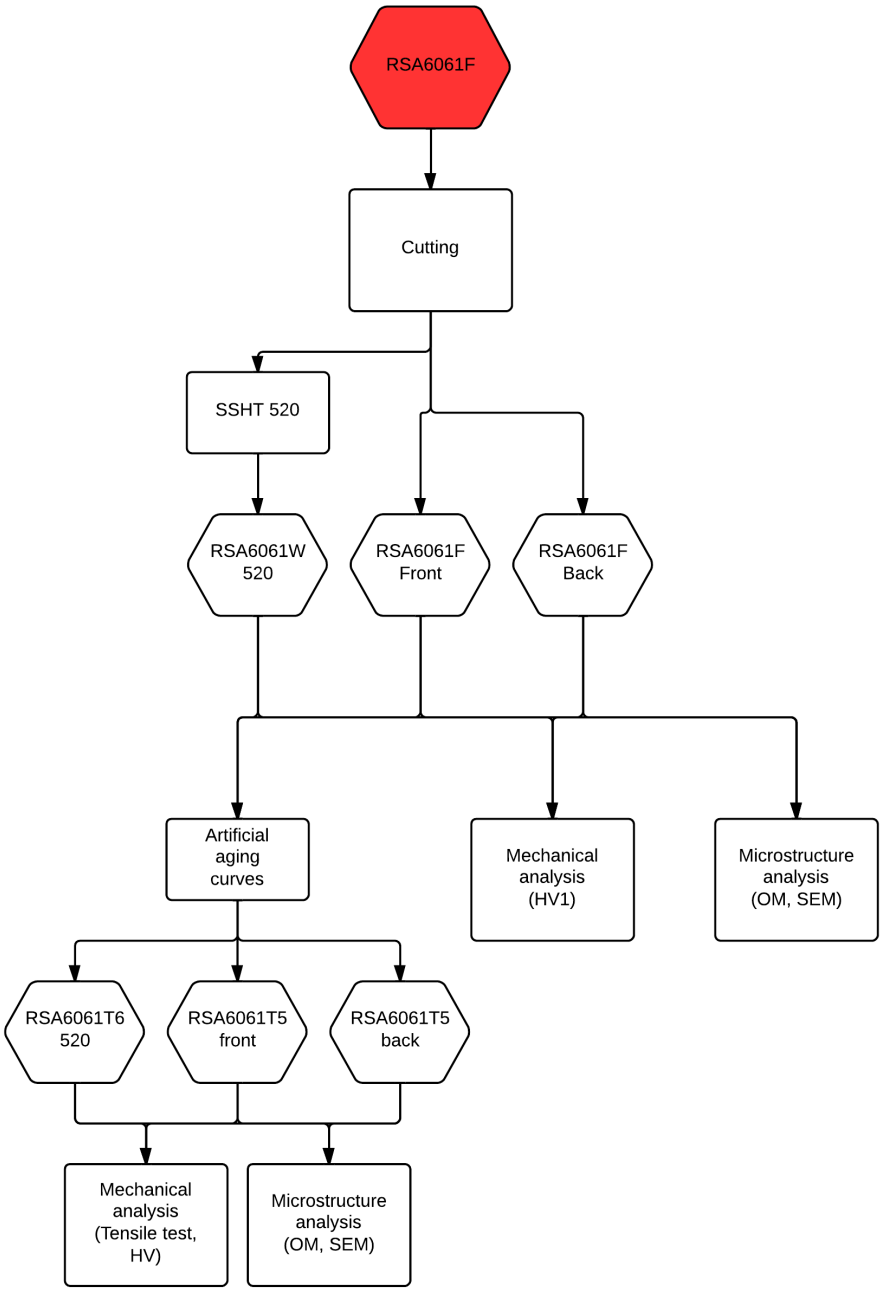

Figure 18: Flow chart of second stage investigations performed on screw extruded profiles. Please not that the starting material was in temper F and the solid solution heat treatment was 520°C

In the last stage investigations, the main issue was to compare the effects of the solid solution heat treatment temperature, i.e. 540, 560 and 580°C, on microstructure and mechanical properties (Figure 19)

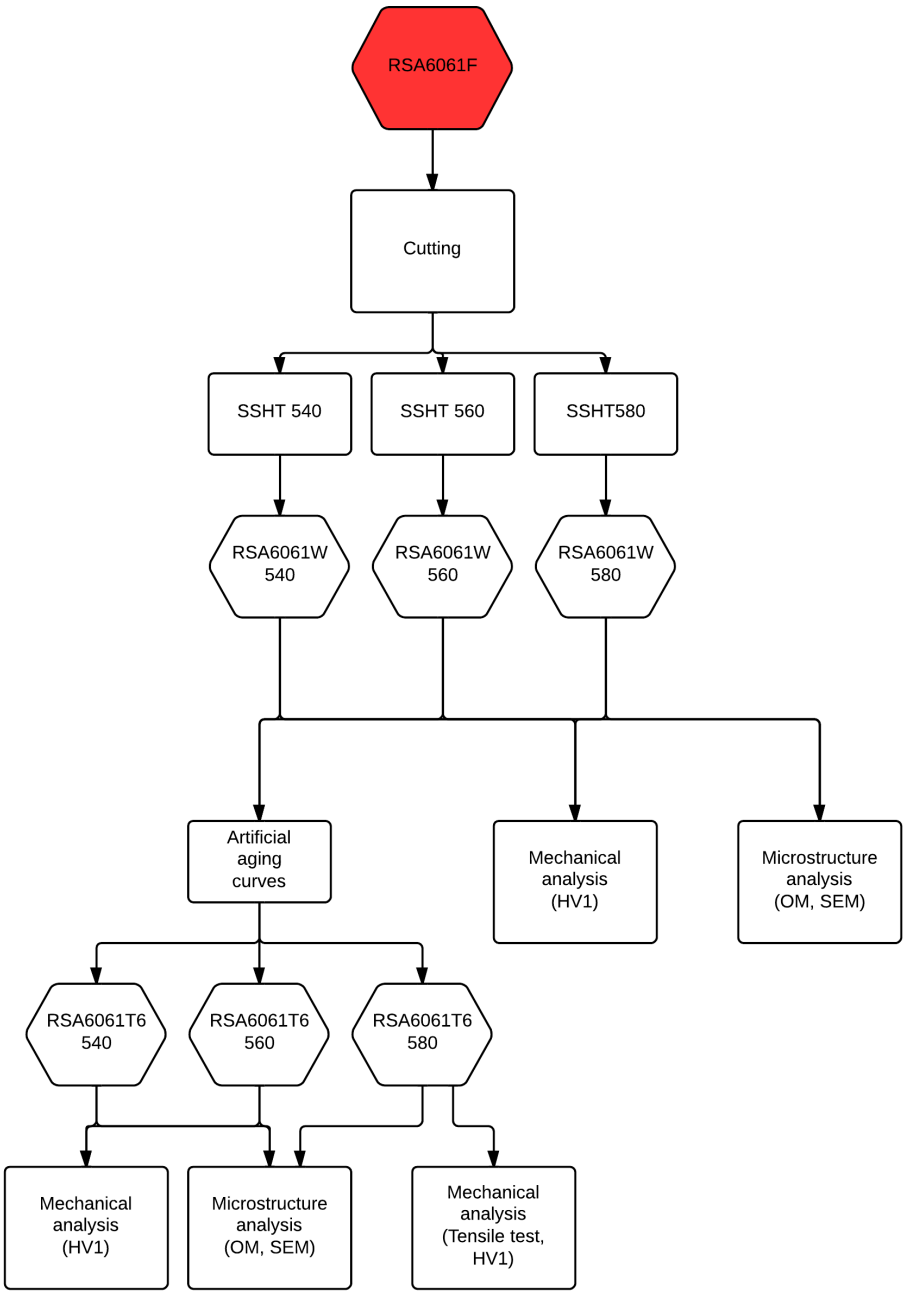

Figure 19: Flow chart of third stage investigations performed on screw extruded profiles in the profile position "back". Solid solution heat treatements 540, 560 and 580°C were compared.

3.5. Cutting of profiles

Due to different properties along the extruded profiles originating from the way they were cut, it was important to cut the profiles the same way to get consistent results. The RSA6061 "Back" is the part that was closest to the die when cut, and RSA6061 "Front" the part furthest away from the die. A schematic drawing of this situation is illustrated in Figure 20.

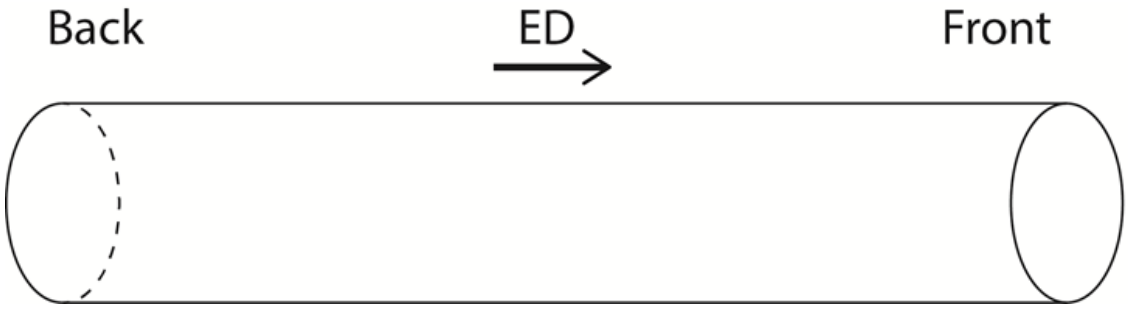

Figure 20: Sketch of profile showing the "Back" and "Front", where "Back" means the position closest to the die. Experiencing the shortest time in air before quenching.

3.5.1. Second stage cutting

In the second stage (Figure 18) of the investigations, the profiles were cut in two different ways, i.e. for the artificial aging curves and for tensile tests. For the artificial aging curves, four centimetres of each end of the profile was cut to four samples, as illustrated in Figure 21. The labelling "RSA6061F Front" was from the front of the extruded profile and "RSA6061F Back" from the back. The samples for SSHT at 520°C followed by artificial aging were taken randomly from the cut profile

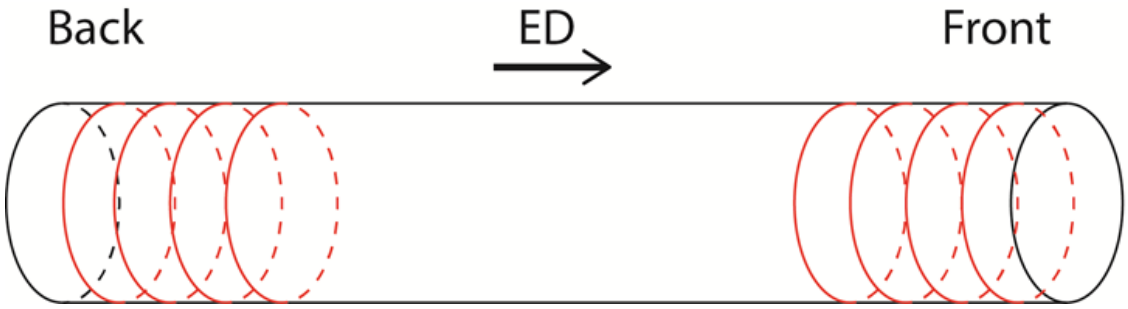

Figure 21: Schematic illustration of the collection of samples for artificial aging.

Moreover the tensile samples for "RSA6061F Front" and "RSA6061F Back" were cut as shown in Figure 22. Likewise the samples for artificial aging, the tensile samples for "RSA6061W 520" were taken randomly from the cut profile

Figure 22: Positions of the tensile tests, i.e. taken in position "Back" and "Front" of profiles.

3.5.1.1 Final cutting before analysis

Samples used in OM or SEM analysis were either cut in cross section or longitudinal section. The cross section samples were cut as seen in Figure 21, while the longitudinal were cut as illustrated in Figure 23.

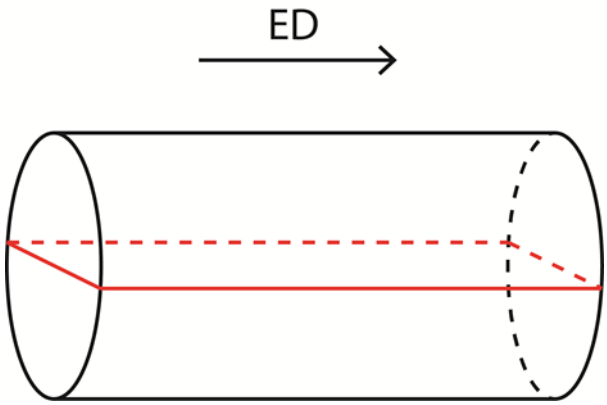

Figure 23: Longitudinal section sample position.

3.5.2. Third stage cutting

In the third stage (Figure 19) the samples for all procedures and analyses were taken from the back of the profiles. The six centimetres of the back were used for SSHT and artificial aging and collected as shown in Figure 24.

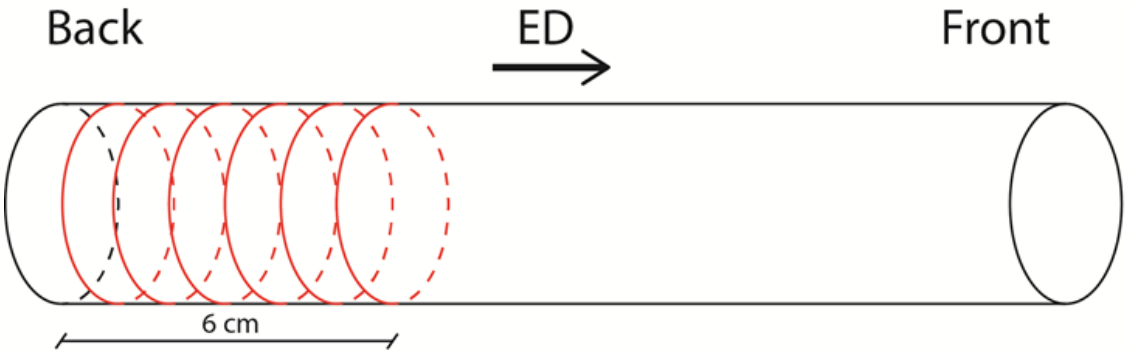

Figure 24: Sample positions for SSHT and artificial aging (in the "Back").

Furthermore, the tensile specimens were cut from the ten centimetres of the back, as shown in Figure 22. While the samples for OM and SEM analysis were cut as in Figure 25. Longitudinal samples were taken as in Figure 23.

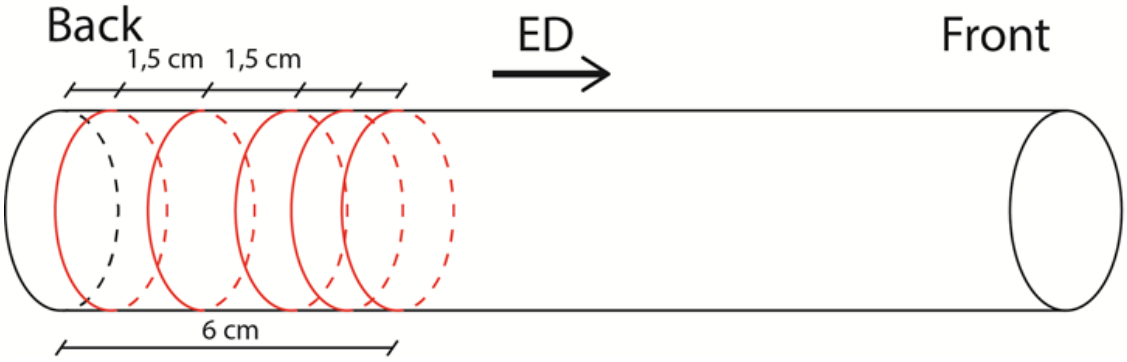

Figure 25: Cutting of profiles for OM and SEM.

3.6. Heat treatment

The heat treatments carried out in both of the last two stages are described in the following.

The solid solution heat treatment was done in a salt bath. The salt bath was set to the desired temperature and controlled by a thermocouple. The samples were held by a steel wire and dipped into the bath. All samples were SSHT for ten minutes and then quenched in room tempered water. The hardness and conductivity was tested within half an hour after quenching. Before the hardness tests, the samples were grinded with 1200 SiC paper, followed by taking five hardness indentations in the centre part of the cross section. Further the conductivity was analysed with Foerster Sigmascope 2.069, conducting five measurements in the same area. The sample labelled RSA6061F, SSHT at 520°C, was heat treated six days after extrusion. The SSHT performed at 540°C, 560°C and 580°C respectively were conducted one month after extrusion.

In order to determine maximum strength, artificial age hardening curves were established. The ageing was performed in an oil bath at 185°C, with the times seen in Table 5. Please note that the age hardening was done 24 hours after solid solution heat treatment. All these samples were placed in the bath at the same time, except for the 10, 20 and 40 minutes sample taken in between other samples for practical reasons. After reaching the desired aging time, samples were quenched in water, grinded with 1200 SiC paper and hardness tested in the centre part of the cross section maximum half an hour later.

Table 5: The selected time for artificial aging at 185°C.

10 min	20min	40 min	1 hr	2 hr	4 hr	5 hr	6 hr	8 hr	1 day	5 days

The heat treatment procedure for obtaining the T6 condition was decided based on the artificial aging curve (section 4.2.4). An overview of all the heat treatments aiming to reach the T6 condition is shown in Table 6.

Table 6: Final heat treatment procedures for obtaining the T6 condition.

	SSHT temperature[°C]	SSHT time [minuts]	Time in RT [hr]	Artificial aging temperature [°C]	Artificial aging time [hr]
RSA6061T5 Front	0	0	0	185	4
RSA6061T5 Back	0	0	0	185	4
RSA6061T6 520	520	10	24	185	4
RSA6061T6 540	540	10	24	185	4
RSA6061T6 560	560	10	24	185	4
RSA6061T6 580	580	10	24	185	8

For convenience the amount of days after extrusion the different heat treatments were done are shown in Table 7.

Table 7: The time after extrusion the various heat treatments were performed.

#days after extrusion	What	Comment
0	Screw Extrusion	Quenched
6	SSHT 520°C	Used for AAC
7	Artificial aging	RSA6061F Front, Back, RSA6061W 520
35	SSHT 520°C	Tensile tests
36	Artificial aging	Tensile tests (RSA6061F Front, Back, RSA6061W 520)
41	SSHT 540°C, 560°C, 580°C	Analysis HV1 and El. Conductivity
60	SSHT 540°C	Used for AAC
61	SSHT 560°C Artificial aging 540°C	Used for AAC
62	SSHT 580°C Artificial aging 560°C	Used for AAC
63	Artificial aging 580°C	Used for AAC

3.7. Mechanical analysis

The procedures for mechanical analysis were the same for the second and the third stage.

3.7.1. Hardness testing

Before Vickers hardness testing the samples was grinded to a 1200SiC paper finish. The testing was performed with "Struers Duramin A2500" or "Matsuzawa DVK-IS", using a load of 1kP (HV1). The distance between indent was at least three times the diameter of the indent.

For establishing the age hardening curves five hardness measurements were conducted on each sample, i.e. randomly at the centre part. It was important to avoid pores/cracks developed during the solid solution heat treatment procedures, since these defects could introduce un-wanted measurements.

3.7.2. Tensile testing

The screw extruded profiles were mechanically tested using standard tensile tests. The profiles were machined at "Finmekanisk verksted" at NTNU. Prior to machining the samples had undergo a minor stretch to be straightened. The sample geometry is given as in Figure 26.

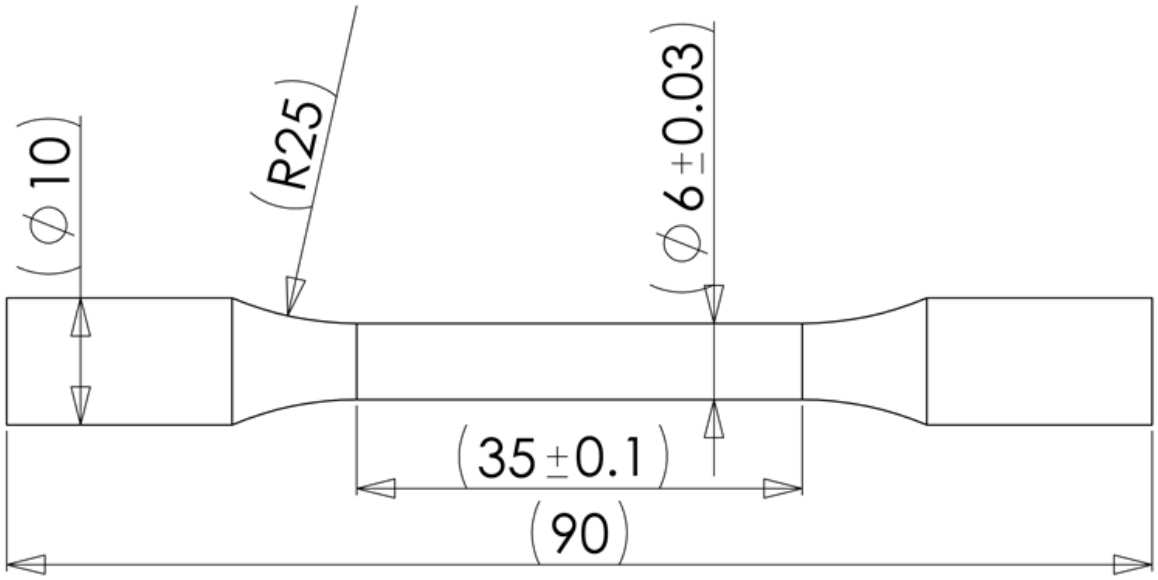

Figure 26: Dimensions [mm] of the tensile test samples.

Three different tests were conducted for each condition of the last two stages. Before testing the actual diameter of sample was measured. All samples were stretched to fracture at a constant stroke displacement rate and strain was monitored using a standard 255mm gauge-length extensometer. The testing machine was a servohydraulic 100kN MTS.

3.8. Microstructure analysis

The microstructure analysis was the same for all stages of the study.

3.8.1. Sample preparation

Samples used for OM and SEM/EDS were cut then embedded in epoxy. They were subsequently grinded by hand or with an automatic grinder following the steps 500, 800, 1000/1200 and 2000/2400 mesh (Struers SiC paper). During grinding the samples were cooled/lubricated by water, and at the 2000/2400 stage, soap was used to prevent SiC particles to attach to the sample. The samples were then polished either by hand or with an automatic polisher with 3µm and 1µm diamond spray. For the samples analysed in respect to Mg_2Si particles, the polishing steps were performed with a lubricant that was ethanol based. This was done to prevent oxidation of Mg when exposed to water.

3.8.2. Optical microscopy (OM)

The optical micrographs were taken with the microscope Leica MEF4M and camera "Jenoptik ProgRes C10 plus". The range of magnifications was from 50X (5X objective lens) to 200X (20X objective lens), depending on the sample and purpose of the picture. The macrographs were taken with bright field contrast, apertures were adjusted for optimum conditions. For anodized samples, a polarizator and sub-

parallel lambda plate were used to obtain grain contrast. The contrast and brightness were subsequently manipulated in Photoshop when needed.

3.8.3. SEM/EDS

The SEM and EDS analysis was done in a Zeiss Supra 55VP, which is a low vacuum field emission SEM. Samples that were embedded in epoxy for grinding/polishing, were dipped in liquid nitrogen to be able to break the epoxy. The samples were then washed in acetone and ethanol before drying. To fasten the samples to the sample holder, a carbon tape was used.

The microscopy was done with secondary electrons (SE) for topography and backscatter electrons (BS) for z-contrast. For the fractography of tensile samples SE were used with a suitable working distance and an acceleration voltage as given on each fractography image.

For the polished samples, all from the longitudinal section, both SE and BS were used. The working distance was 10mm and the acceleration voltage 9eV, i.e. to get traces of all alloying elements of interest and as possible emission depth as small. The EDS analysis was used to detect different elements, either with a point scan on particles or an area scan over the aluminium matrix.

3.9. Particle and grains size analysis

3.9.1. Particle analysis

The particle analysis was done with ImageJ. To quantify dispersoids micrographs with magnification of 5000X was used and to quantify Mg_2Si particles, 1000X magnification was used.

To quantify the particles, several steps of image manipulation had to be done. First the picture had to be an 8-bit grey scale, and then the contrast and brightness had to be corrected. To determine which “colour” that should be counted, the threshold had to be set. An example before and after this procedure is shown in Figure 27.

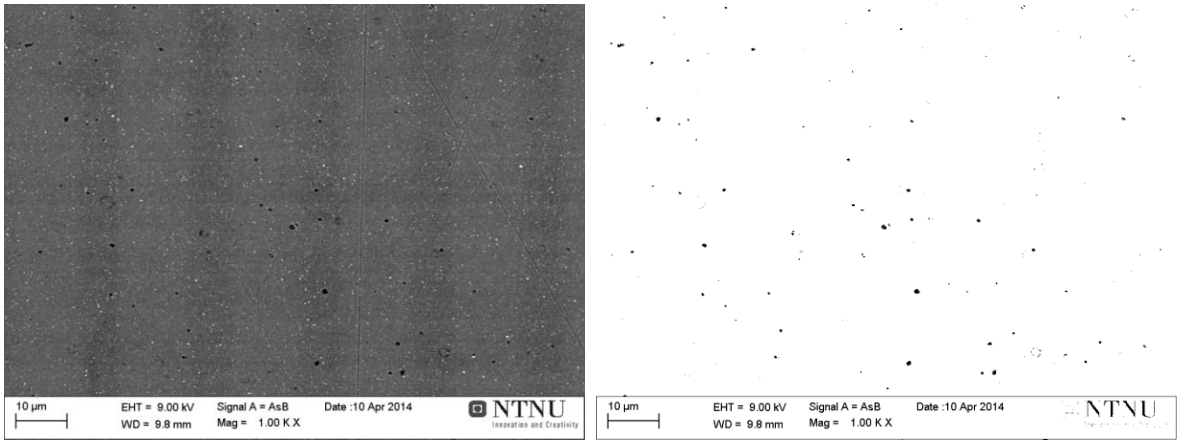

Figure 27: Before (left micrograph) and after (right micrograph) manipulation of Mg_2Si particle analysis.

Then the particles (black dots) were counted with the "particles analysis" tool in ImageJ. The minimum particle size was set manually to get rid of "noise". In several pictures there were numerous one to three pixelsized "particles" and these were excluded from the counting. Subsequently, data were loaded into Excel and sorted with the "Frequency" function, i.e. counting the number of particles between two or more determined values. An example of the parameters used for this procedure is shown in Table 8. The particle size shown as particle diameter (d), calculated from the measured area (A) of the particles. Moreover the particles were assumed to be circular and the diameter was calculated using: $d = 2 * \sqrt{\frac{A}{\pi}}$.

Table 8: Example of the frequency function parameters.

Particle values	Set values	Count
1		1 [value under 1.9]
2	1.9	2 [value between 1.9 and 2.9]
2	2.9	1 [value over 2.9]
3		

3.9.2. Grains size analysis

The grain size was measured on anodized sample micrographs, transvers to the longitudinal section. *ImagJ* was used to manipulate the colour and Excel was used to count the number of grains from the line scan data. For each micrograph there was five line scans having a length of approximately 10mm. To get grain contrast, the colours were manipulated from *RGB Color* (255 colours) to *8-bit Colors* with four colours (Figure 28). By this one could get one colour per grain. By drawing a straight line with the *line tool* and using the *Plot Profile* tool, the colour code per pixel made it possible to count the number of grains. With *Excel* and the macro (Appendix A), the number of grains was counted. Then the number of grains was divided by the length of the line, i.e. to get the average grain size. The average of five line scans and obtained standard deviations were here used. Please not that "grains" having one pixel width were not counted.

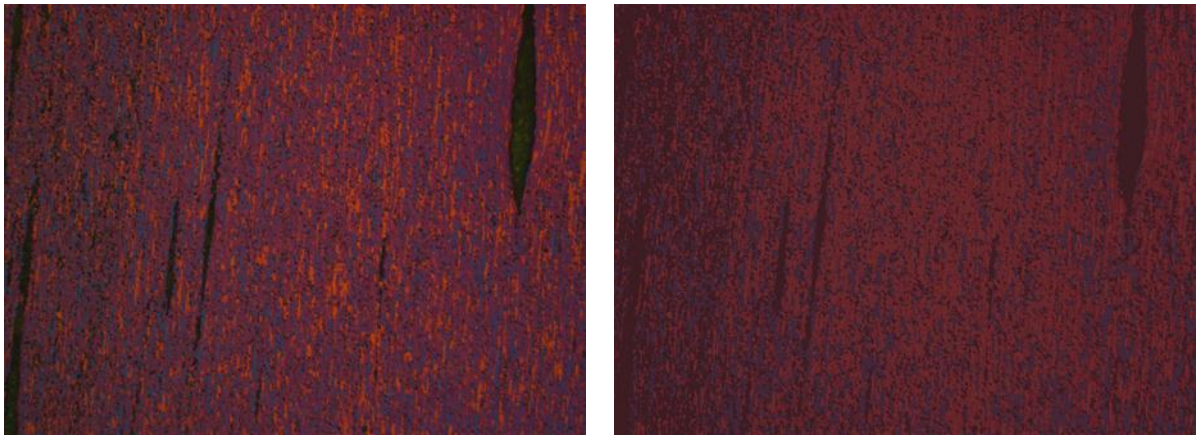

Figure 28: Before (left) and after (right) colour manipulation.

3.9.3. Quantifications of cracks and recrystallized zone

Cracks and the recrystallized zone were studied on longitudinal optical micrographs in the transvers direction. There were five measurements taken using *ImageJs* line and measure tool. The averages values of these were used.

4. Results

In this the results from the study are illustrated and described, starting with the RSP6061 granules followed by extruded profile. Note that the EDS analysis (section 4.3) describes all particle analysis in this study.

4.1. RSP6061 granulates

The RSP6061 granulates were analysed with secondary and backscatter electrons in the SEM. An overview of a polished granule is shown in Figure 29. The rough parts of the sample were not grinded/polished, but the blank parts (left side of granule) were polished and investigated.

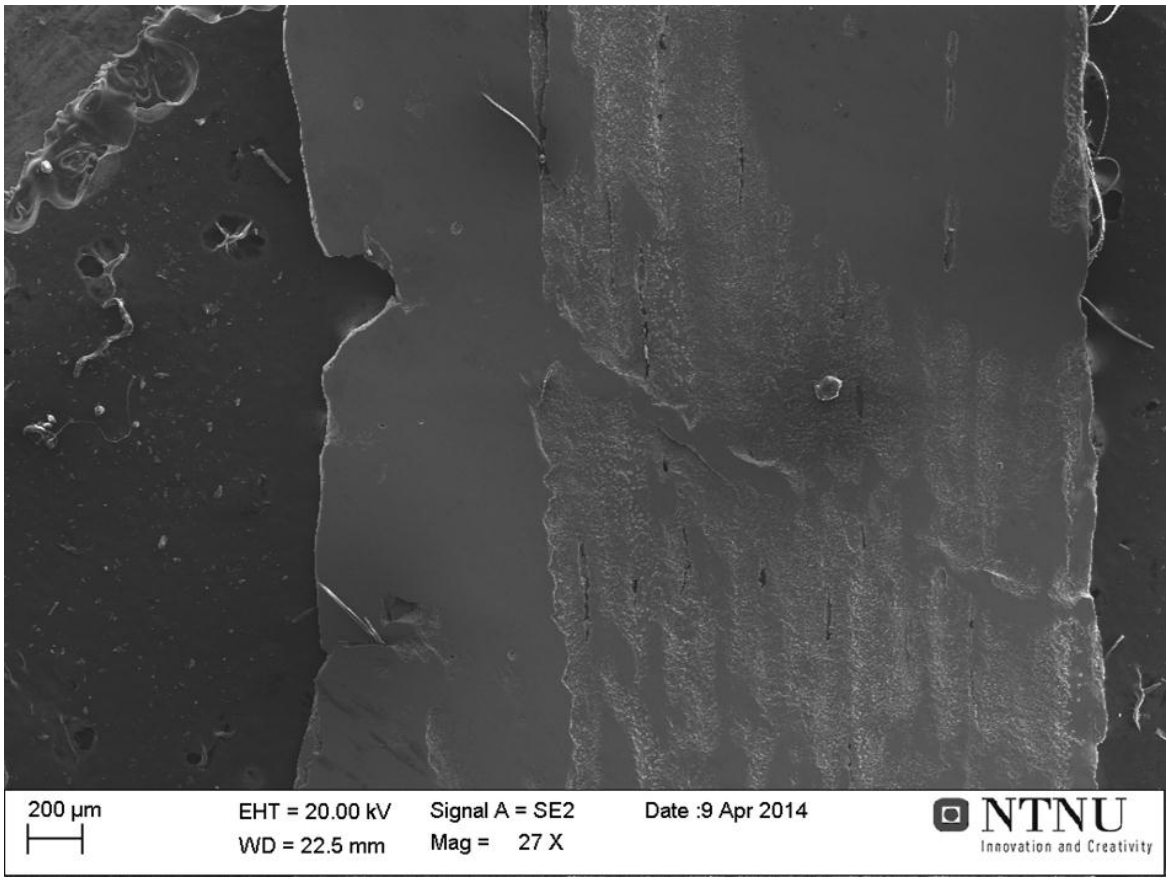

Figure 29: Overview of RSP6061 granule with SE.

At a magnification of 5000X (Figure 30) black spots and many smaller white spots that believed to be dispersoids. The dispersoids were quantified and the corresponding particles size distribution is showed in Figure 31. This revealed a bi-modal distribution, i.e. one spanning from ~40nm to 80 nm and the other between ~80nm-150nm. However, few large particles/dispersoids could also be observed (~0.2µm in diameter).

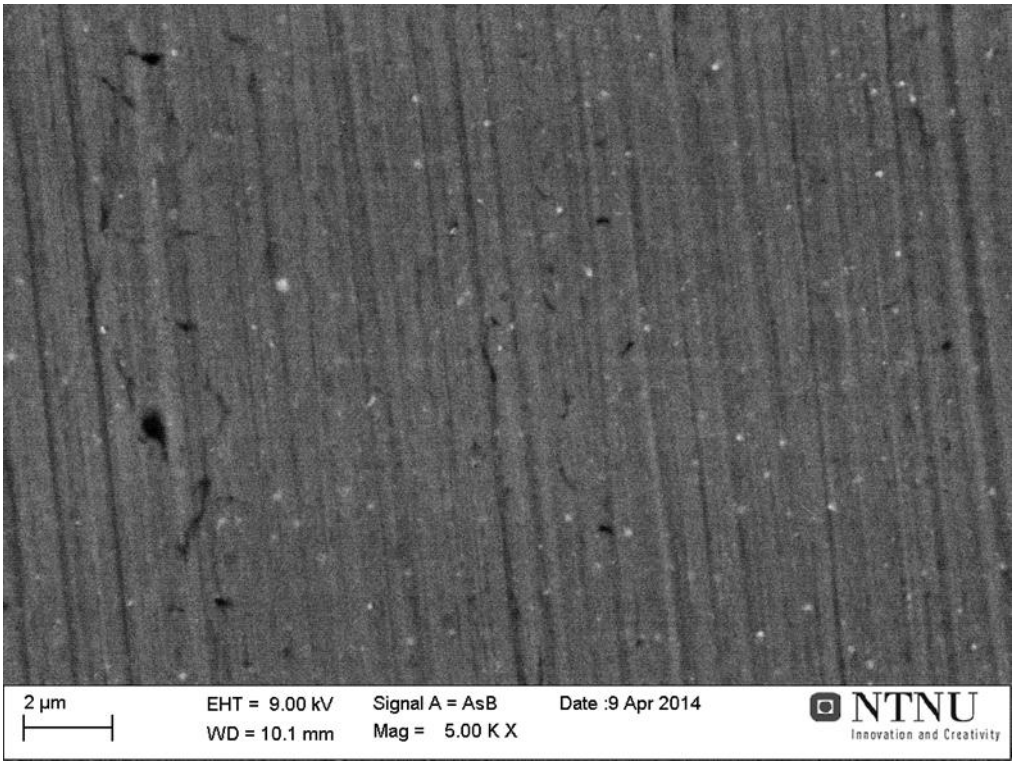

Figure 30: SEM backscatter micrograph of RSP6061 granule. The white particles are probably dispersoids.

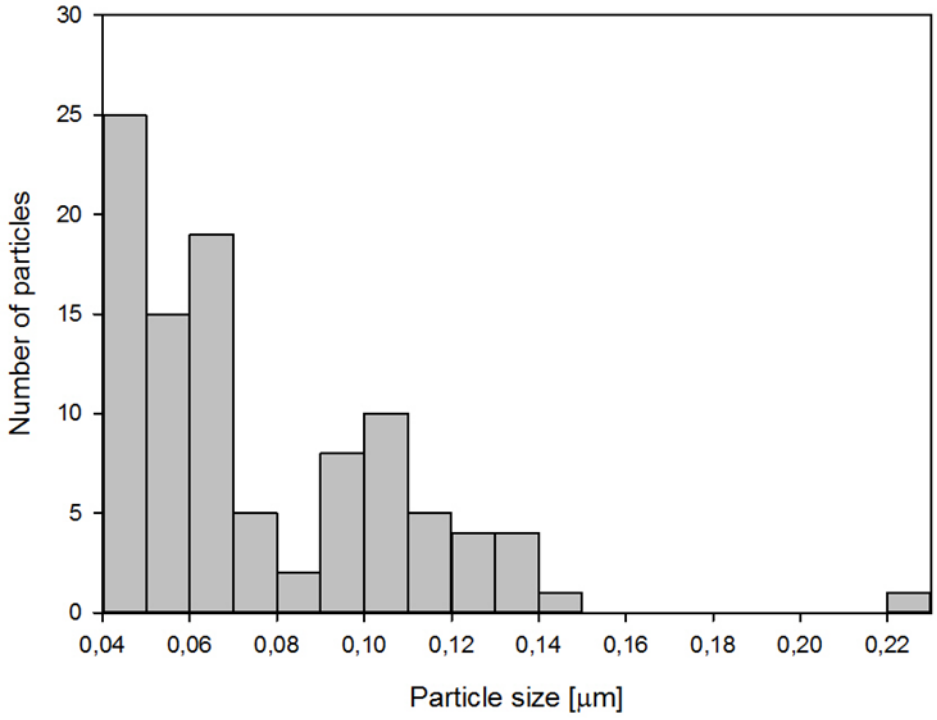

Figure 31: Particle distribution of RSP6061 obtained in the SEM.

4.2. Extruded profile

In Figure 32, four extruded profiles are shown. The profiles were successfully extruded without any defects, such as blisters. The bends on the profile comes from the cutting process during extrusion, and a notch from the bolt cutter can be seen on each profile (right side).

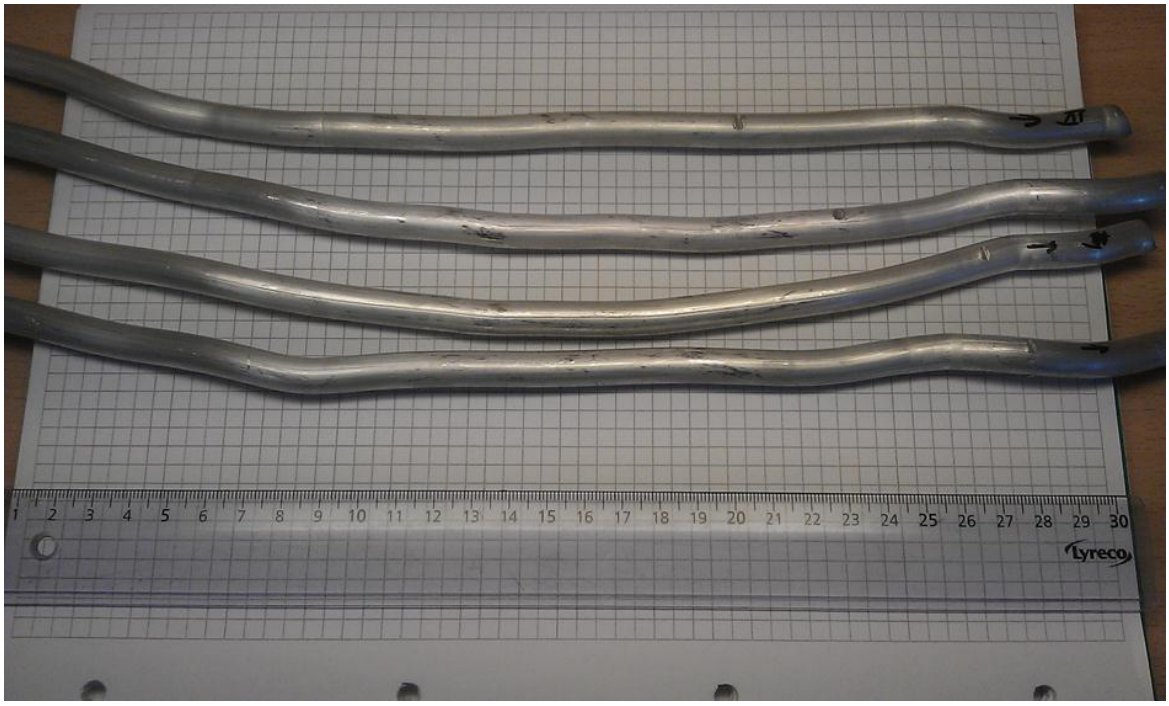

Figure 32: Extruded profiles having 10mm diameter. Extrusion direction is from left to right.

4.2.1. Extrusion speed

An estimate of the extrusion speed from six profiles is given in Table 9. Here the average and standard deviation numbers are in bold. As one can see, the average speed was 1.15±0.2cm/s

Table 9: Extrusion speed data based on length and time measurements.

	Profile 1	Profile 2	Profile 3	Profile 4	Profile 5	Profile 6	Average	SD
Length [cm]	36.0	37.5	33.5	36.0	38.5	33	**35.8**	**1.86**
Time [s]	32.4	32.5	23.2	33.8	29.2	41.4	**32.1**	**5.41**
Extrusion speed [cm/s]	1.11	1.15	1.44	1.07	1.32	0.81	**1.15**	**0.20**

4.2.2. As extruded profiles

4.2.2.1 Hardness

The hardness of an extruded profile was measured to see if the hardness was consistent through the thickness of the samples. The obtained hardness values of the cross section and the longitudinal section are shown in Figure 33. The graphs show that there is no clear tendency of a different hardness at the surface versus the centre. The measurements in obtained in the two sections were also fairly consistent.

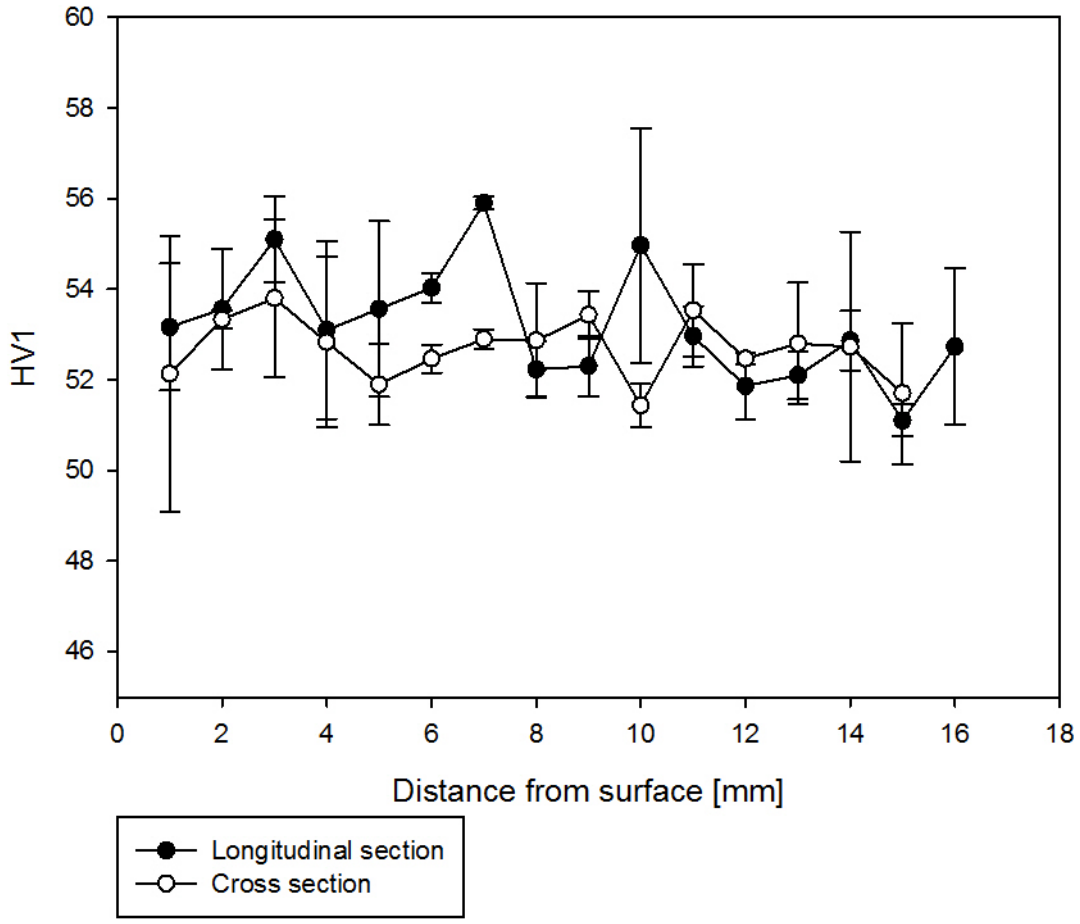

Figure 33: Hardness of as extruded RSA6061F, longitudinal and cross section, as function of the distance from surface.

4.2.2.2 OM

In Figure 34 and Figure 35 the longitudinal sections of the RSA6061F Back and Front. The micrograph is merged from 12 separate micrographs, with 50X magnification. Note the black stripes, which are grinding stripes.

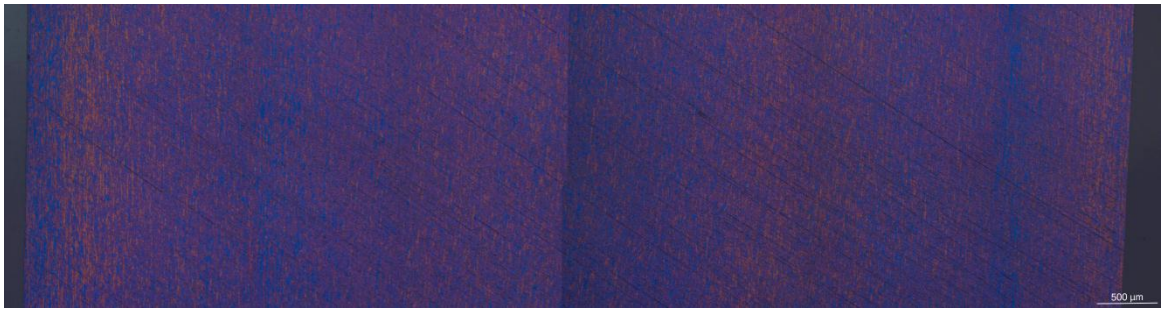

Figure 34: Longitudinal section of RSA6061F Back.

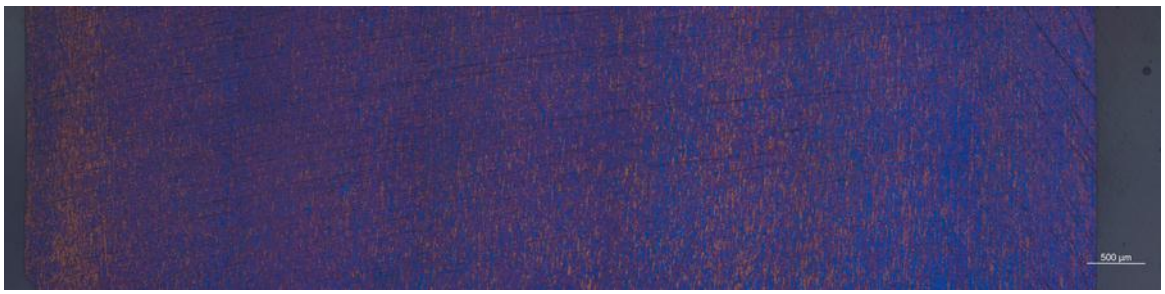

Figure 35: Longitudinal section of RSA6061F Front.

The measured grain size of RSA6061 F, Front and Back are shown in Table 10. The grain size and standard deviation is fairly bigger in the Front than in the Back.

Table 10: Grain sizes of RSA6061F Back and front.

	Grain size [µm]	SD
RSA6061F Back	7.4	0.2
RSA6061F Front	7.9	0.6

4.2.2.3 SEM

In Figure 36 and Figure 37 the backscatter micrographs of the RSA6061F (as extruded state) are shown. Black particles (Mg_2Si) and white particles (dispersoids) can be observed. Mark that there are some grinding and polishing strikes on the micrographs, i.e. preparation was not perfect. The micrographs to the left, were used for Mg_2Si analysis and the right ones were adopted for dispersoid analysis.

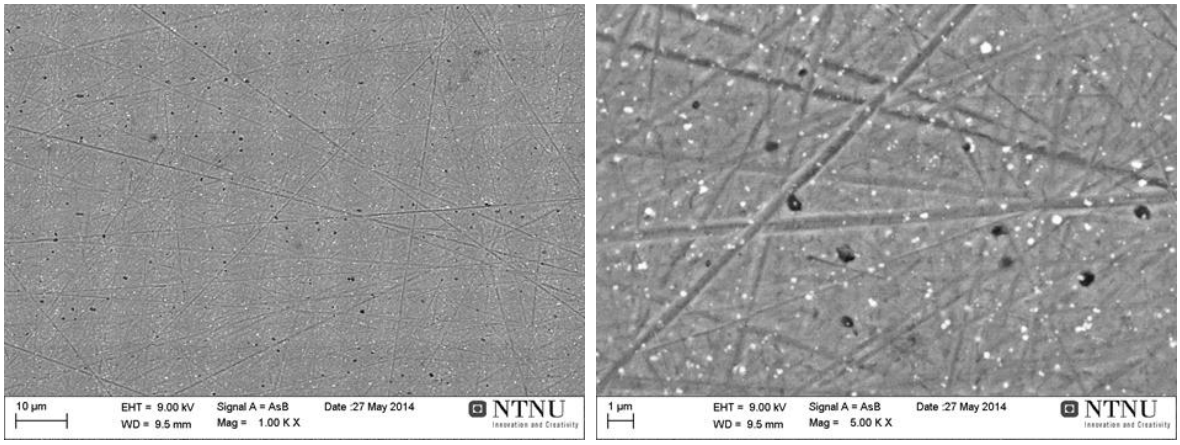

Figure 36: SEM backscatter images of as extruded RSA6061F Back, in longitudinal section.

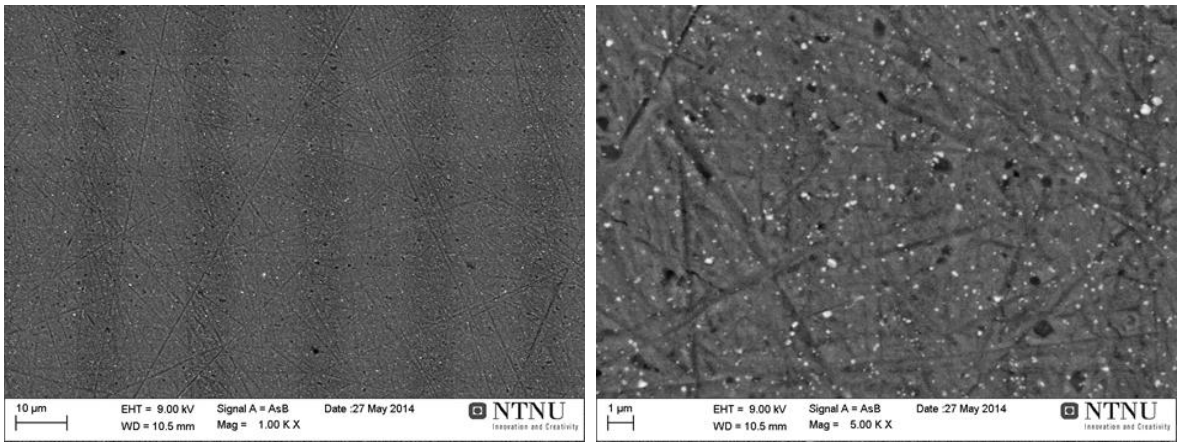

Figure 37: SEM backscatter image of as extruded RSA6061F Front, in longitudinal section.

The particle distribution of Mg_2Si and dispersoids are shown in Figure 38. It can be observed that RSA6061 F Back has less smaller Mg_2Si, but more larger ones than the RSA6061 F Front. Moreover the dispersoid distribution shows that RSA6061 F Front had generally more dispersoids than RSA6061F Back.

Mg_2Si **Dispersoids**

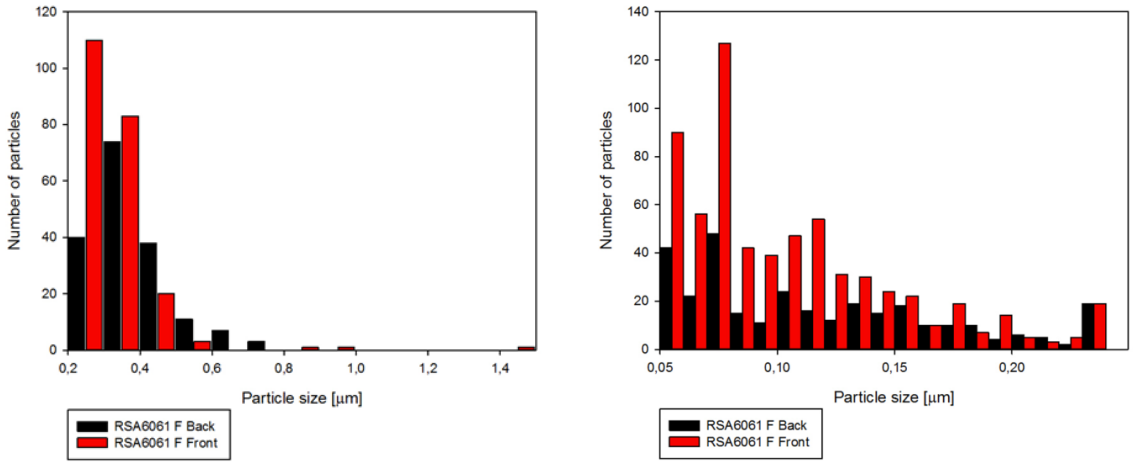

Figure 38: Mg_2Si (left) and dispersoids (right) size distribution of as extruded RSA6061 F.

4.2.3. Solid Solution Heat Treated Material

4.2.3.1 Effect of SSHT on hardness and electric conductivity

The effect on hardness and electric conductivity from the four different SSHT temperatures is shown in Figure 39 and Figure 40. The hardness was highest for SSHT temperature 520°C, while consistent for the three temperatures. The standard deviation is increasing for increasing temperature (displayed by the error bars). The electric conductivity was decreasing with increasing temperature, the electric conductivity is 20% lower for SSHT temperature 580°C than 520°C.

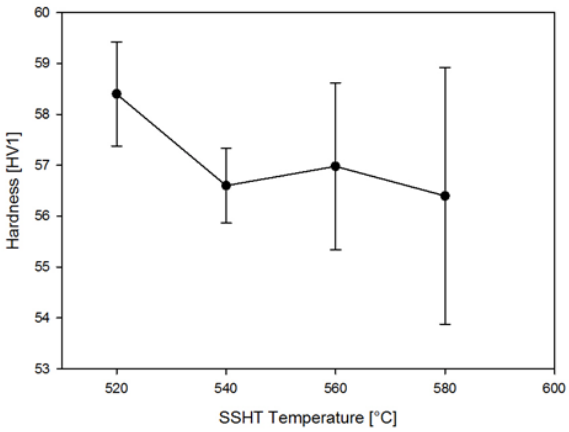

Figure 39: Influence of SSHT temperature on hardness.

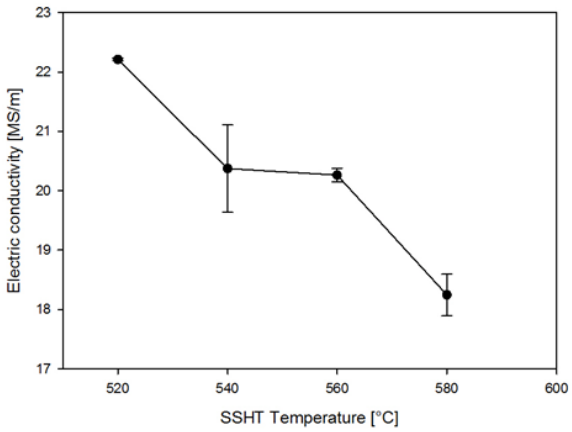

Figure 40: Electrical conductivity as function of SSHT temperature.

4.2.3.2 Optical microscopy

In Figure 41 the optical micrograph of the longitudinal section of RSA6061W 520 is shown. The measuring bar is 500µm. Note the small recrystallized grains in the upper left corner.

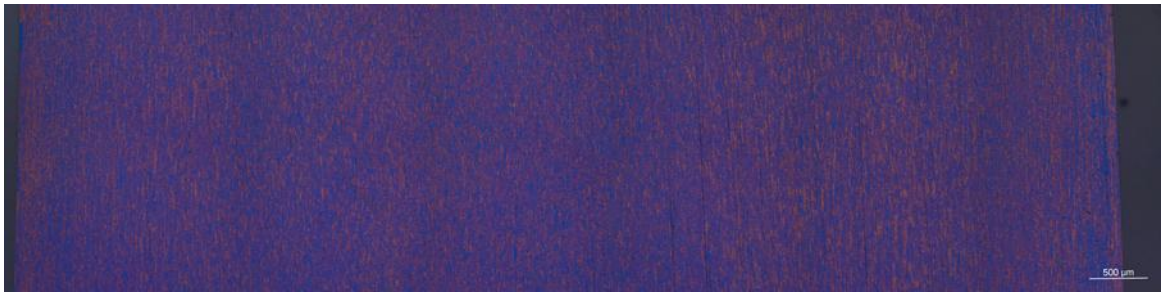

Figure 41: Optical micrograph of the longitudinal section of RSA6061W, SSHT temperature 520°C

The longitudinal section of RSA6061W 540°C is shown in Figure 42. The micrograph shows a homogenous grain size without any pores or recrystallized zone.

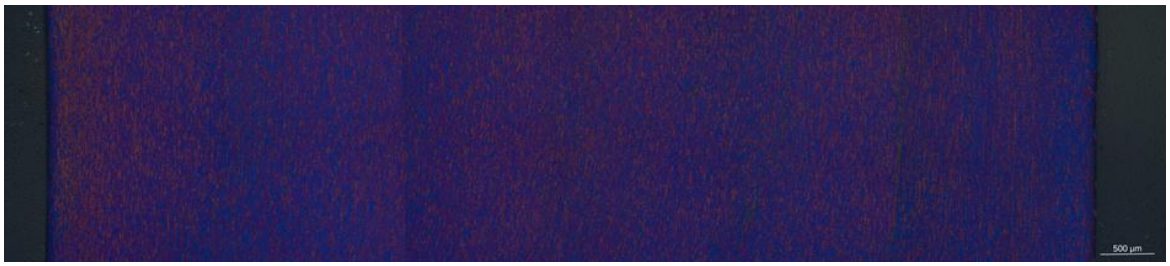

Figure 42: Microstructure of RSA6061W, SSHT temperature 540°C.

The microscopy of RSA6061W 560°C, seen in Figure 43, had a recrystallized zone at the surfaces and pores through the thickness of the sample.

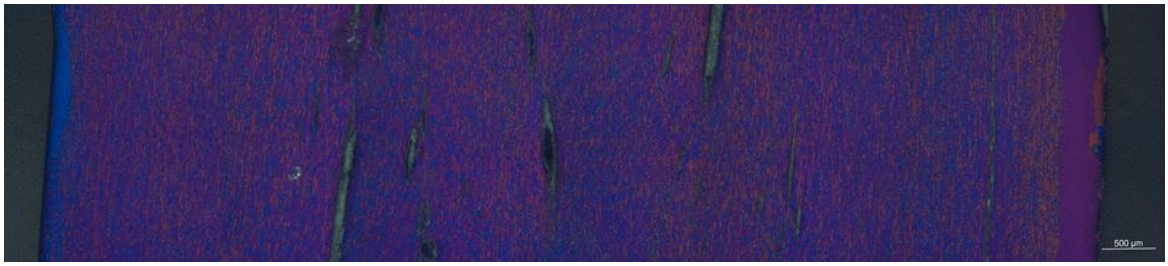

Figure 43: Microstructure of RSA6061W, SSHT temperature 560°C.

The RSA6061W solutionized at580°C (Figure 44) had the same tendency as RSA6061 560°C, e.g. having a recrystallized zone at the surface and pores through the thickness of the sample.

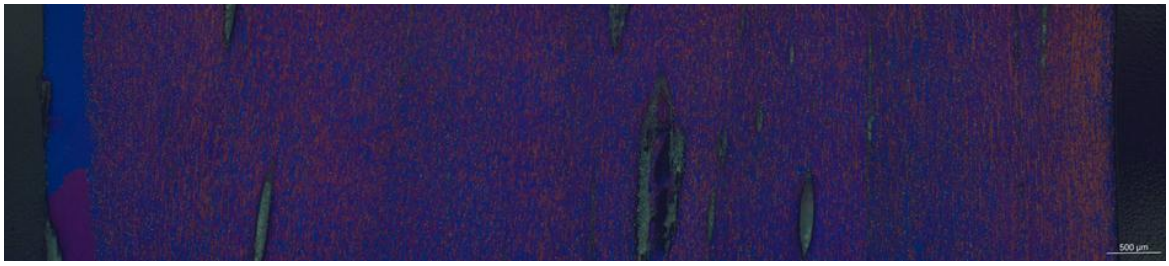

Figure 44: Microstructure of RSA6061W, SSHT temperature 580°C.

The measured grain sizes shown in Table 11 indicate that the grain size was almost the same for all SSHT temperature. There was a small increase in grain size with increasing temperature, while the standard deviation was fairly constant.

Table 11: Grain size in RSA6061W profiles as a function of SSHT temperature.

	Grain size [µm]	SD
RSA6061W 520	6.4	0.4
RSA6061W 540	6.3	0.2
RSA6061W 560	6.7	0.4
RSA6061W 580	6.8	0.4

Further, the crack width size in the SSHT profiles is shown in Table 12. Note that that a SSHT of 520°C and 540°C appeared without cracks, where 560°C and 580°C introduced cracks with increasing magnitude, with increasing temperature.

Table 12: Crack width sizes for RSA6061W profiles as function of SSHT temperature.

	Crack size [µm]	SD
RSA6061W 520	0	0
RSA6061W 540	0	0
RSA6061W 560	107	18
RSA6061W 580	130	26

Also the width of the recrystallized zones was measured as function of the SSHT temperature (Table 13). The RSA6061W 560 had recrystallized zones on both sides, but with different width. However, RSA6061W 580 had a recrystallized zone only on the left side.

Table 13: Width of recrystallized zone as function of SSHT temperature.

	Recrystallized zone [µm]	SD
RSA6061W 520	34	11
RSA6061W 540	0	0
RSA6061W 560 left side	169	24
RSA6061W 560 right side	409	32
RSA6061W 580 left side	393	30

4.2.3.3 SEM analysis

The results from backscatter analysis after various solution heat treatments can be seen in the figures below (Figure 45 to Figure 48). Black particles (Mg_2Si) and white particles (dispersoids) can be seen. To determine the amount of Mg_2Si the magnification of 1000X was used. There was a clear tendency towards zero Mg_2Si when the SSHT temperature increased. The dispersoids were analysed at 5000X magnification, and there was no visible difference in quantity versus the SSHT temperature.

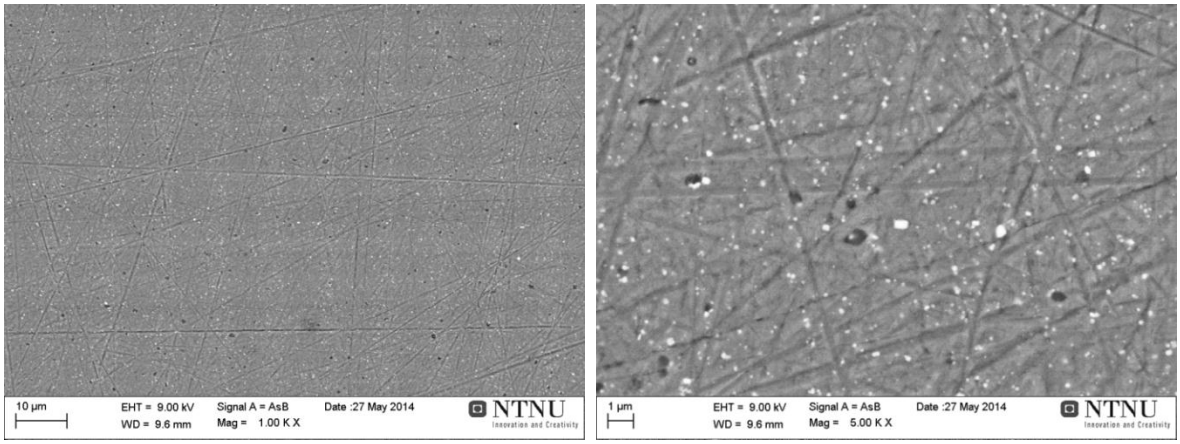

Figure 45: Backscatter micrograph of RSA6061W 520, 1kX to the left and 5kX to the right.

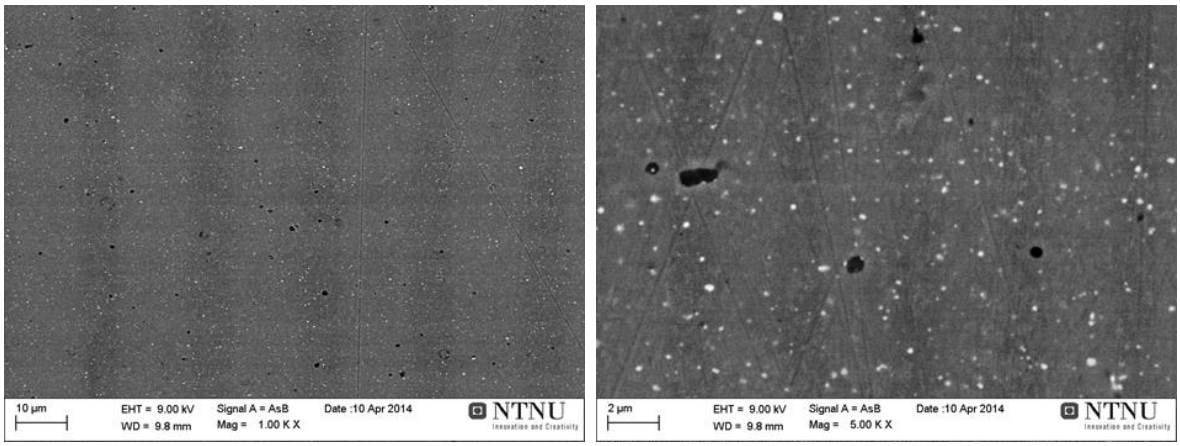

Figure 46: Backscatter micrograph of RSA6061W 540, 1kX to the left and 5kX to the right.

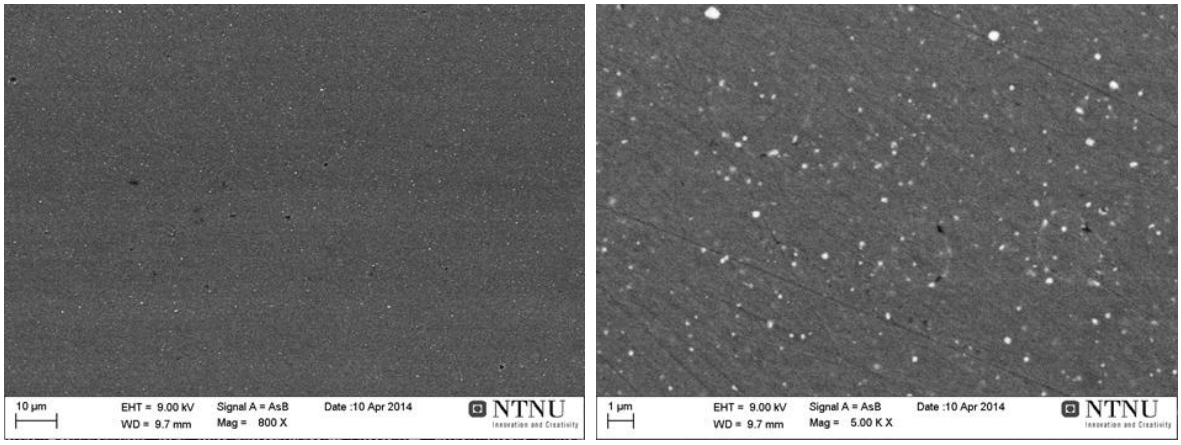

Figure 47: Backscatter micrograph of RSA6061W 560, 800kX to the left and 5kX to the right.

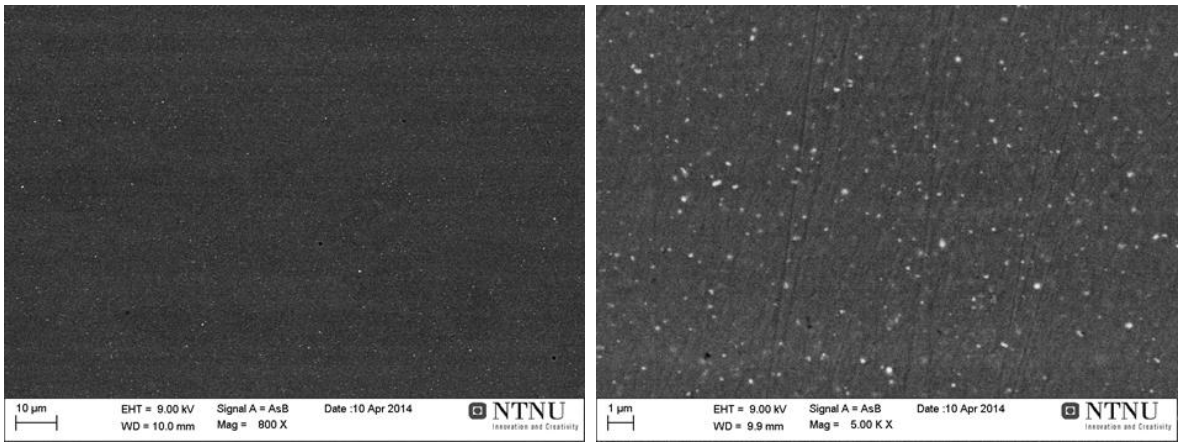

Figure 48: Backscatter micrograph of RSA6061W 580, 800X to the left and 5kX to the right.

In Figure 49 the measured amount of Mg_2Si and dispersoids are shown. For all SSHTs there are large quantities of the smallest Mg_2Si particles (between 0.2µm and 0.3µm). The amount of these particles decreased with increasing particle size. However, the lowest solutionizing temperature (520°C) introduced the largest amount of the smallest Mg_2Si particles. In the size range 0.3-0.5µm, the number of particles increased with decreasing temperature. The dispersoids had no clear distribution, but please note that the three columns to the right are bigger than 0.23µm, i.e. not being between 0.23 µm and 0.24 µm. Please note that the magnification on Figure 47 and Figure 48 are different from the two prior. Therefore the Mg_2Si count in Figure 49, for SSHT temperature 560 and 580, are converted to 1000X magnification "count".

Mg_2Si **Dispersoids**

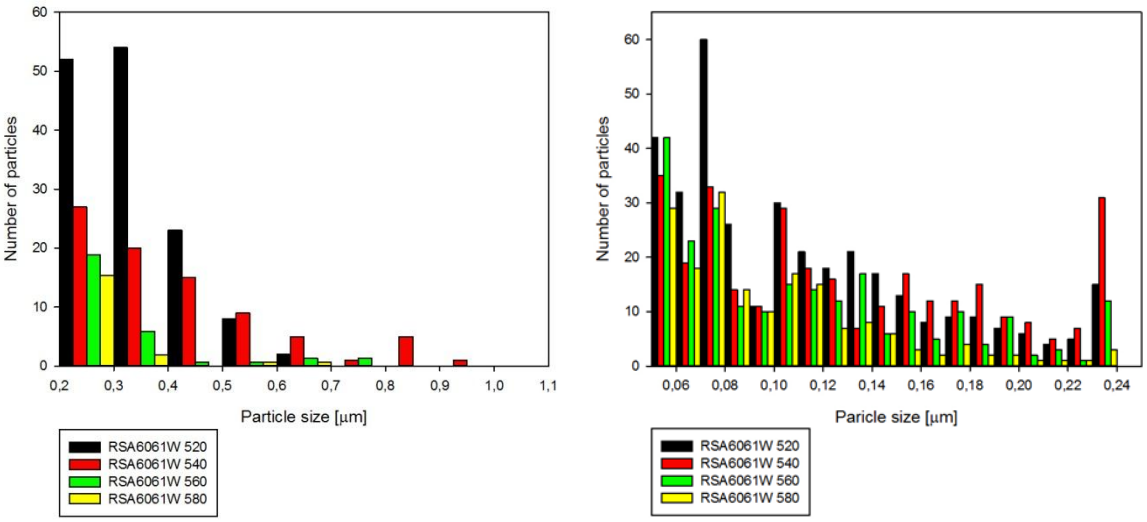

Figure 49: Mg2Si (left) and dispersoid (right) distributions versus SSHT temperature (520°C-580°C).

4.2.4. Artificial aging (185°C)

The as extruded and SSHT profiles were artificially aged and the artificial aging curves are shown below. In Figure 50 the curves for T5 are shown, and there was a significant difference on the response of artificial aging. The RSA6061F Back showed a quite typical effect of aging, with a clear max hardness. The RSA6061F Front showed only a minor response of aging and an untypical increase in hardness after five days. Generally, the "back" position had a higher hardness than the "front" for the as-extruded condition (temper F). Also, the former had a much more rapid aging response.

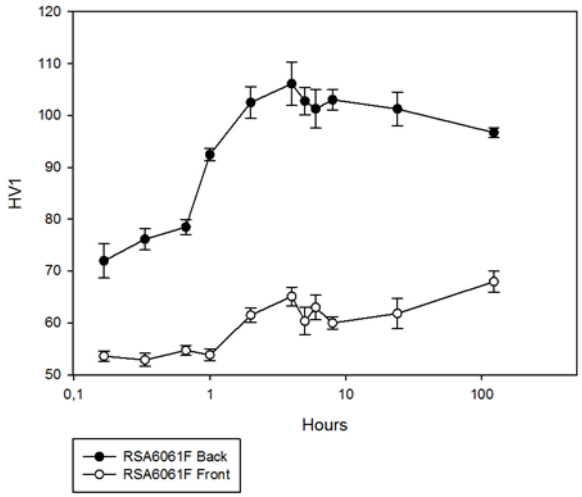

Figure 50: Artificial aging curves for RSA6061F (as extruded condition) comparing the front and back positions.

The SSHT samples had a higher increase in hardness than the “as extruded”, but all appeared with a maximum of ~112HV1. The maximum strength of RSA6061W 520 was at artificial aging of four hours, with a small decrease in strength thereafter. The RSA6061W 540 had the same tendency. RSA6061W 560 showed two tops of maximum strength, one at two hours and one at eight hours and a dip in strength in between. It is important to note that the standard deviation of these strengths were higher than the rest. The RSA6061W 580 had a maximum strength at eight hours, and please note, that the standard deviation was generally higher than for the other temperatures.

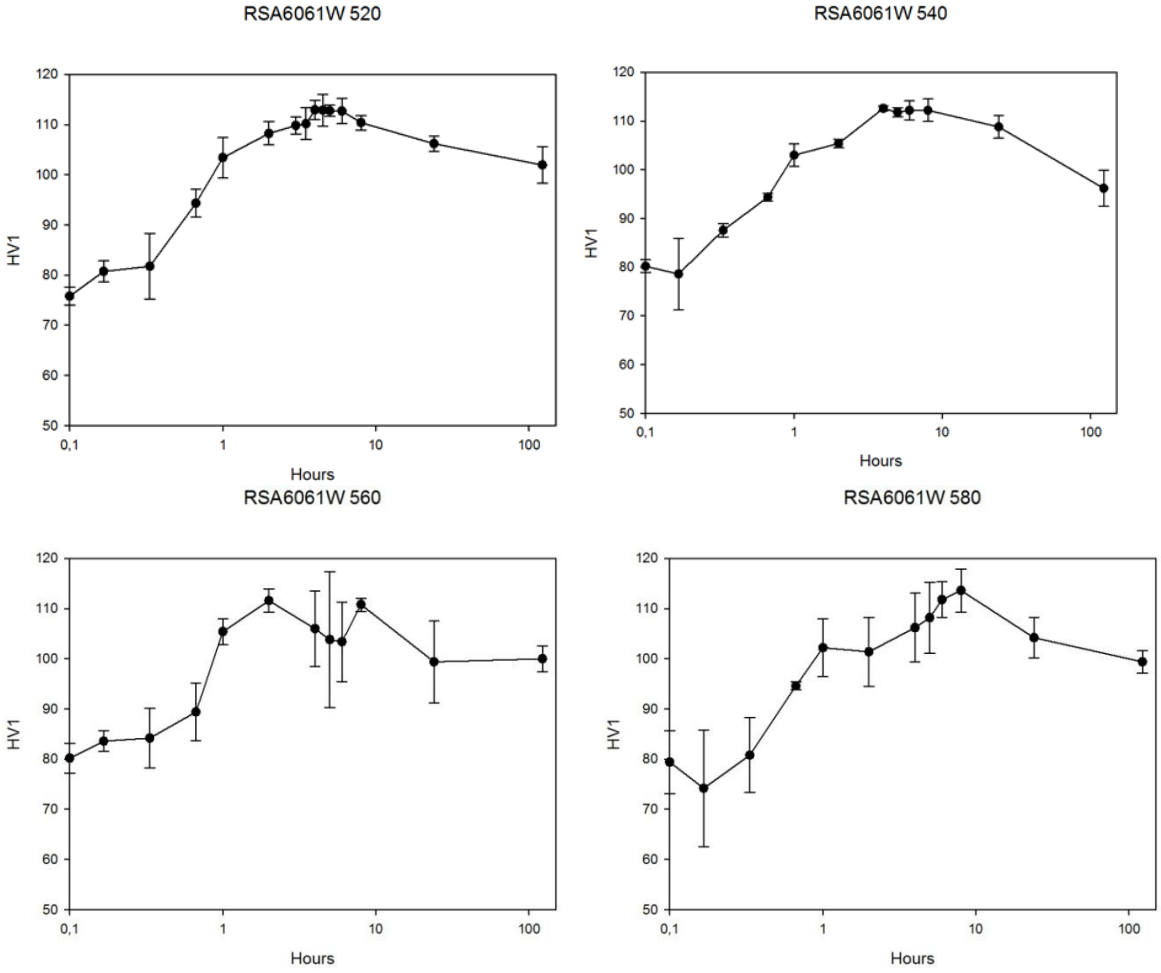

Figure 51: Artificial aging curves at 185°C for RSA6061W after SSHT at 520, 540, 560 and 580°C.

4.2.5. Effect of age hardening on microstructure

In this section the effect of age hardening on microstructure is shown on the as extruded and solid solution heat treated samples.

4.2.5.1 Optical microscopy

Through Figure 52 and Figure 53, the longitudinal section of the profiles heat treated to maximum strength is shown. The RSA6061 T5 grain sizes are displayed in Table 14 and show a grain size with a very small difference, only 0.2 µm. However, this difference was inside the standard deviation for both samples. The grain size

though the thickness was homogenous and there were no cracks or pores in the T5 conditions.

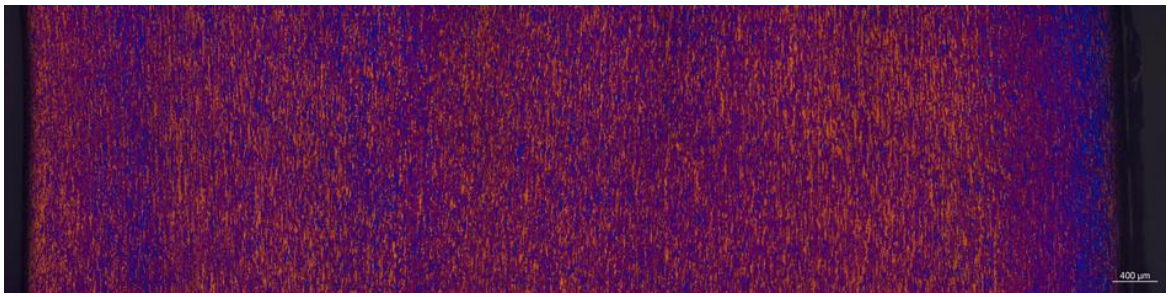

Figure 52: OM of RSA6061 T5 Front, measuring bar is 400µm.

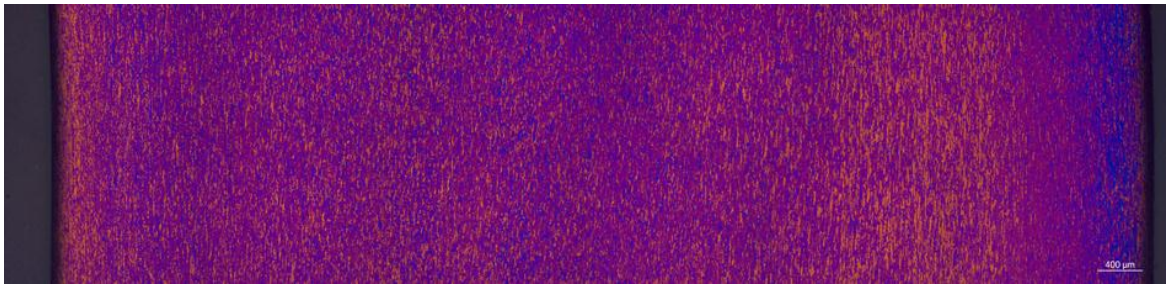

Figure 53: OM of RSA6061 T5 Back, measuring bar is 400µm.

Table 14: Grain sizes of RSA6061 T5, comparing the front and back positions.

	Grain Size [µm]	Standard Deviation
RSA6061 T5 Front	6.1	0.4
RSA6061 T5 Back	6.3	0.2

However, the T6 samples solutionized at 520-580°C (Figure 54 to Figure 57) had all cracks, with a varying amount. From the figures below it seems like RSA6061 T6 520 and RSA6061 T6 580 had the most cracks, but due to observations throughout this study, this is not the case. It was observed that higher SSHT temperature give more cracks. There were also recrystallized zones in RSA6061 T6 560 and 580, and the widest in RSA6061 T6 580.

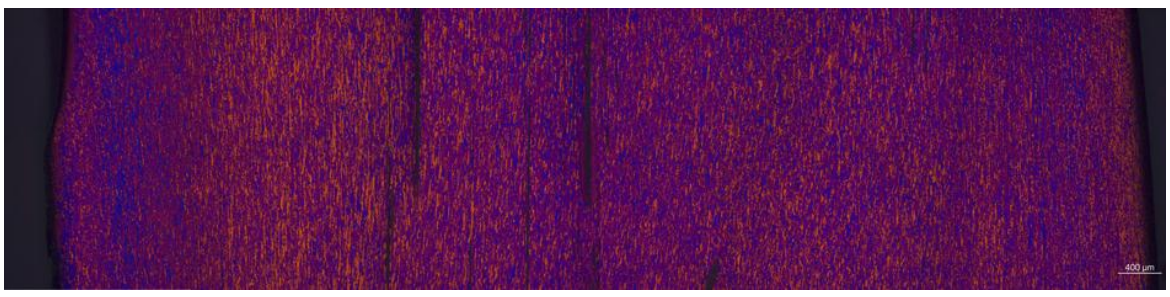

Figure 54: OM of RSA6061T6 520, measuring bar is 400µm, SSHT at 520°C.

Figure 55: OM of RSA6061 T6 540, measuring bar is 500µm, SSHT at 540°C.

Figure 56: OM of RSA6061 T6 560, measuring bar is 500µm long, SSHT at 560°C.

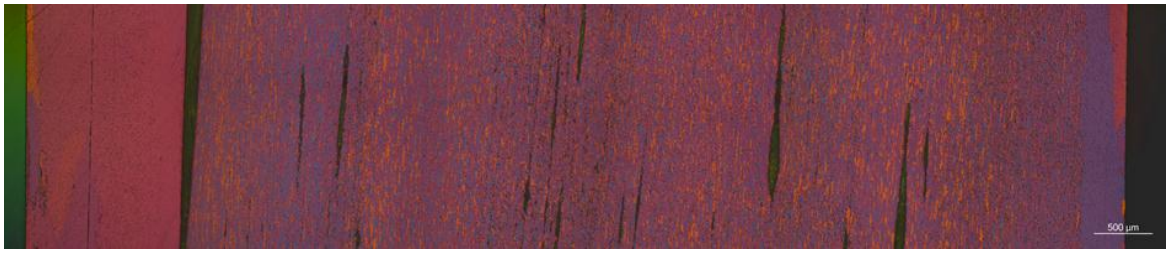

Figure 57: OM of RSA6061 T6 580, measuring bar is 500µm, SSHT at 580°C.

In Table 15 the measured grain sizes for the T6 samples are displayed. The grain size was increasing with increasing SSHT temperature and the standard deviation was close to equal for all heat treatments, except for RSA6061 T6 580, which had a higher standard deviation.

Table 15: Grain sizes of RSA6061 T6, versus SSHT temperature

	Grain Size [µm]	SD
RSA6061 T6 520	6.6	0.7
RSA6061 T6 540	6.6	0.2
RSA6061 T6 560	7.5	0.4
RSA6061 T6 580	7.7	0.7

The maximum crack width sizes are shown in Table 16, i.e. being the biggest cracks observed in the respective samples.

Table 16: Maximum crack width size of RSA6061 T6 samples, versus SSHT temperature.

	Crack width Size [µm]	SD
RSA6061 T6 520	30	4
RSA6061 T6 540	26	3
RSA6061 T6 560	89	3
RSA6061 T6 580	105	21

Moreover, the measurements of the recrystallized zones widths are shown in Table 17. Note the recrystallized zone in RSA6061 T6 580 left side, which was ~25% of the sample thickness.

Table 17: Recrystallized zone width of RSA6061 T6 samples, as function of the SSHT temperature.

	Recrystallized zone width [µm]	SD
RSA6061 T6 520	0	0
RSA6061 T6 540	0	0
RSA6061 T6 560	252	5
RSA6061 T6 580 Left side	1346	15
RSA6061 T6 580 Right side	378	9

4.2.5.2 SEM

In Figure 58 and Figure 59 the backscatter micrographs of RSA6061 T5 are shown (comparing position "back" and "front"). The 1000X magnification was to determine the amount of Mg_2Si (black particles). The 5000X magnification was used for determine the amount of dispersoids (white particles).

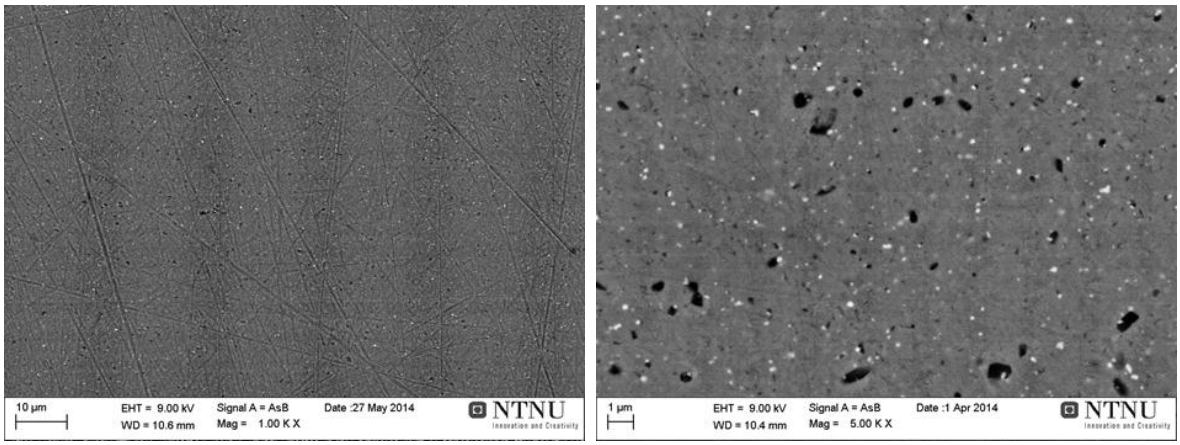

Figure 58: Backscatter images of RSA6061T5 Front, 1kX to the left and 5kX to the right.

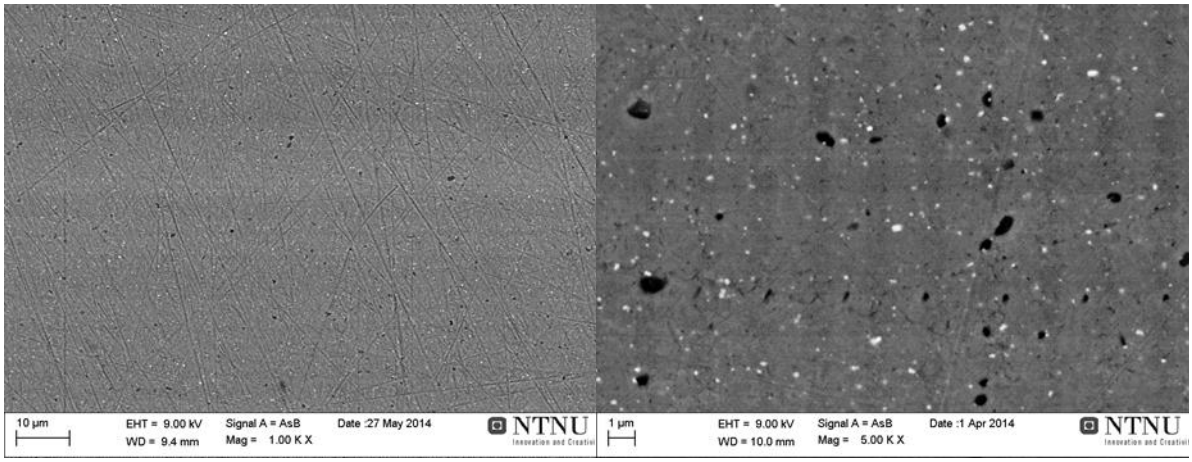

Figure 59: Backscatter images of RSA6061T5 Back, 1kX to the left and 5kX to the right.

The size distribution of Mg_2Si and dispersoids are illustrated in Figure 60. The quantity of Mg_2Si is generally higher for "back", than for the "front" section. Both increase quantity with increasing particle size. The dispersoid distribution does not show a clear tendency, but both front and back seems to have almost the quantity for each size distribution.

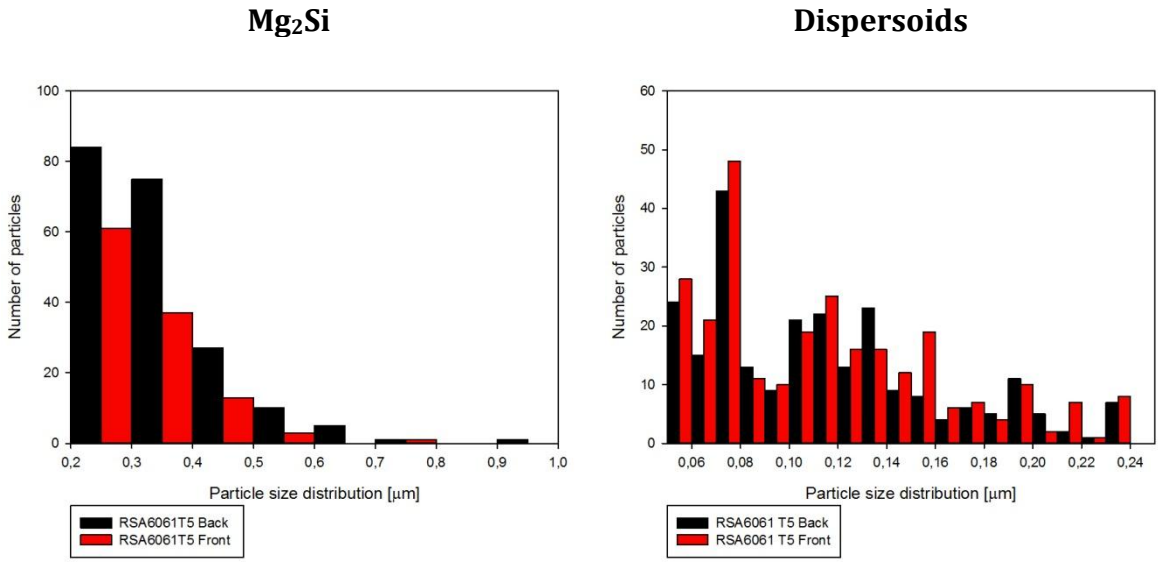

Figure 60: Size distribution of Mg2Si (left) and dispersoid (right) distribution in RSA6061 T5.

In Figure 61 to Figure 64 the backscatter micrographs of the T6 samples are shown. One can observe that the amount of Mg_2Si was getting lower when the SSHT temperature increases. The amount of dispersoids did not have a clear distribution tendency by looking at the micrographs.

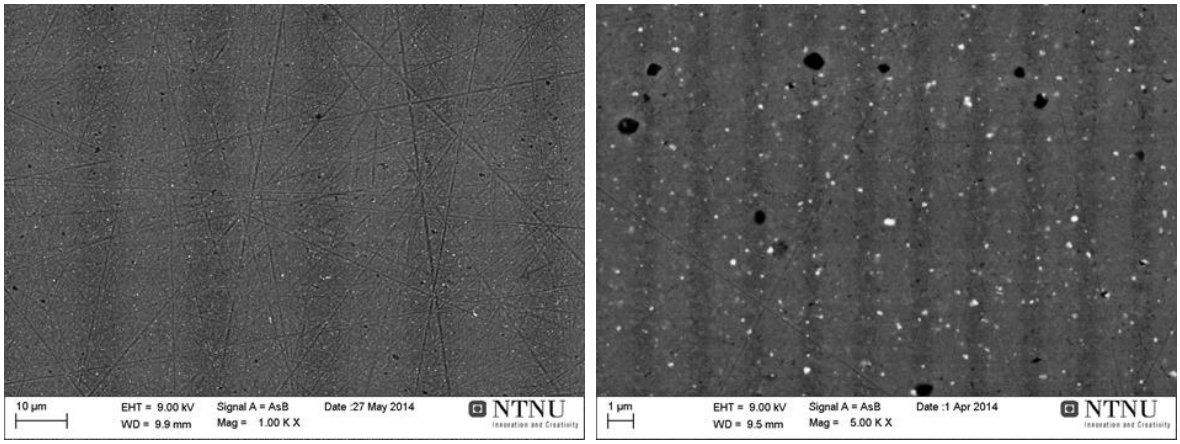

Figure 61: Backscatter images of RSA6061T6 520, i.e. solutionized at 520°C and aged to T6.

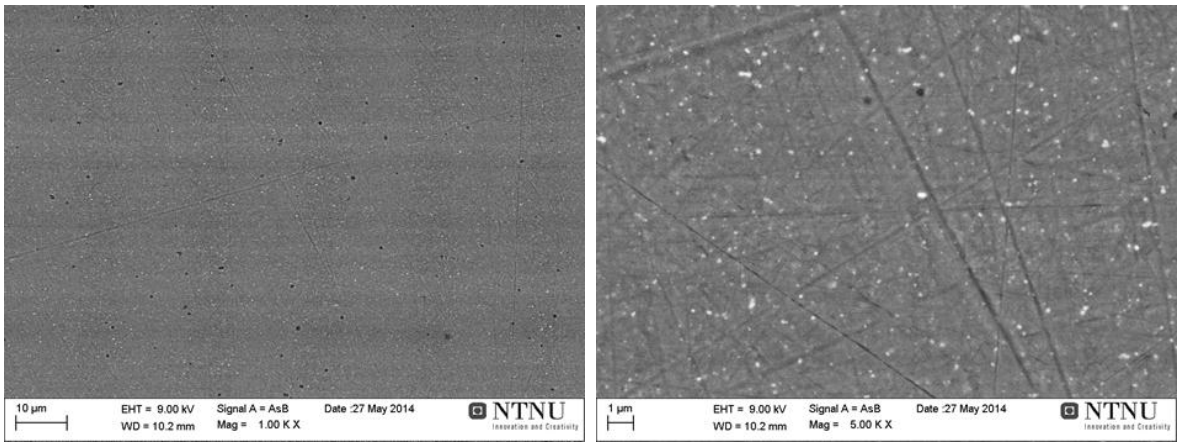

Figure 62: Backscatter images of RSA6061T6 540, i.e. solutionzied at 540°C and aged to T6.

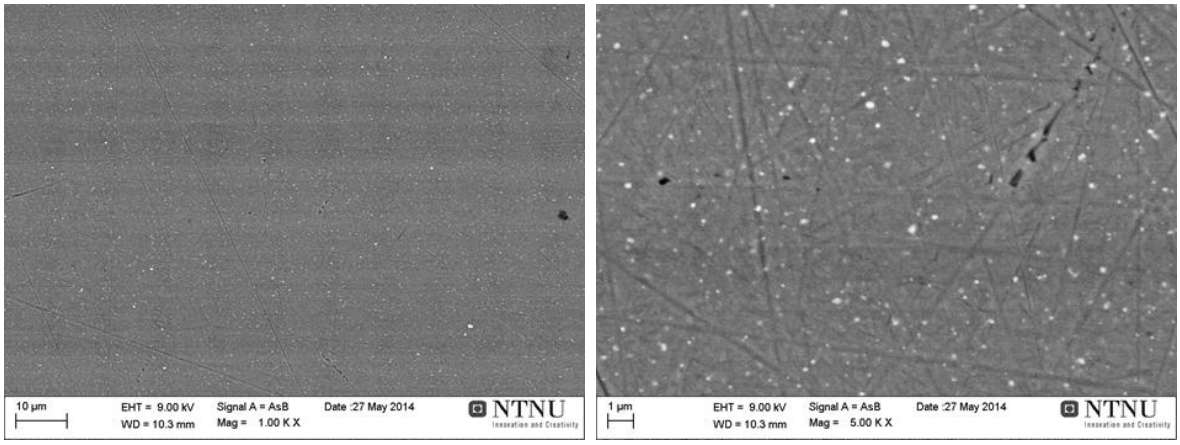

Figure 63: Backscatter images of RSA6061T6 560, i.e. solutionzied at 560°C and aged to T6.

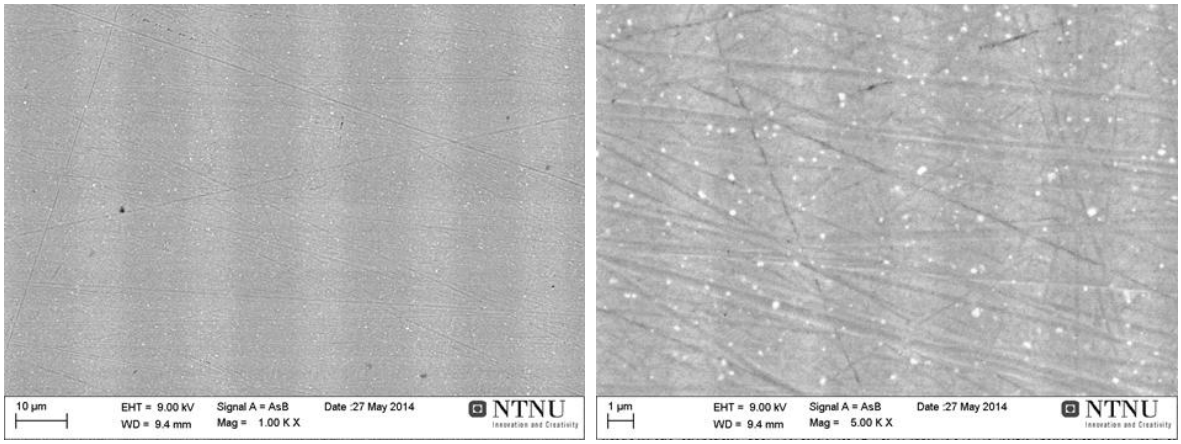

Figure 64: Backscatter images of RSA6061T6 580, i.e. solutionzied at 580°C and aged to T6.

The particle count analysis in Figure 65 shows the same as observed in the micrographs. This means that the amount of Mg_2Si was highly determined by the SSHT temperature. The dispersoid count does not have the same clear tendency.

Mg_2Si **Dispersoids**

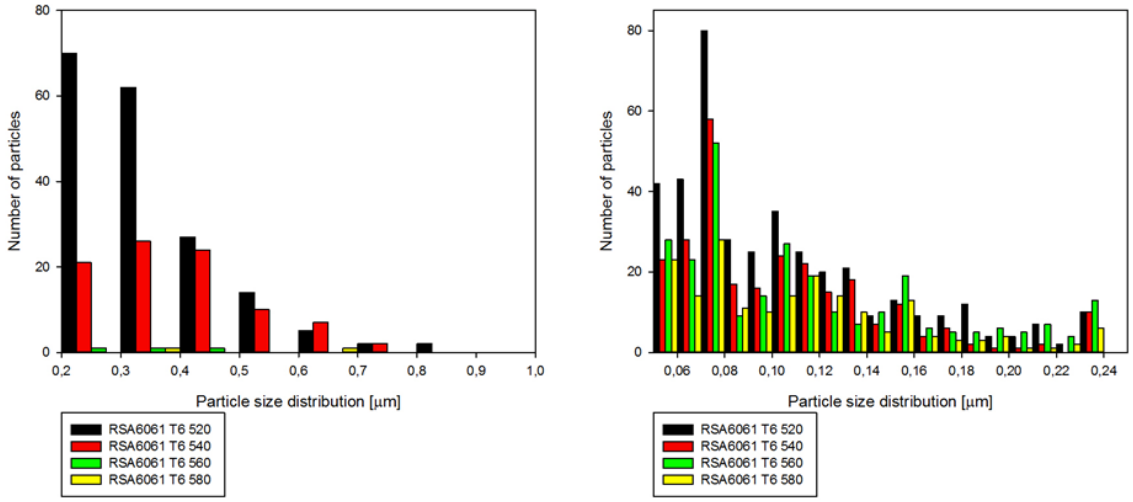

Figure 65: Mg_2Si (left) and dispersoids (right) distribution in RSA6061 T6 versus SSHT temperature.

4.2.5.3 Tensile tests

The results from the tensile tests are shown in the following figures. Here there were three samples for each heat treatment. The axis scales are the same for all graphs except for RSA6061 T6 580 where the x-axis spans up to 0.035 instead of 0.25.

For the RSA6061 T5 Front (Figure 66), all three tensile tests were successful, and some variation in the strength and strain could be observed. The RSA6061 T5 Back (Figure 67) was not successfully monitored after UTS, because the extensometer knife fell in to the necking. So the elongation cannot be seen out of these three samples. There was a clear difference in yield strength and UTS for the front and back of the profiles, i.e. RSA6061T5 Back are the strongest. Note, the ductility of

RSA6061T5 Back cannot be concluded, because of the extensometer knife fell in to the necking.

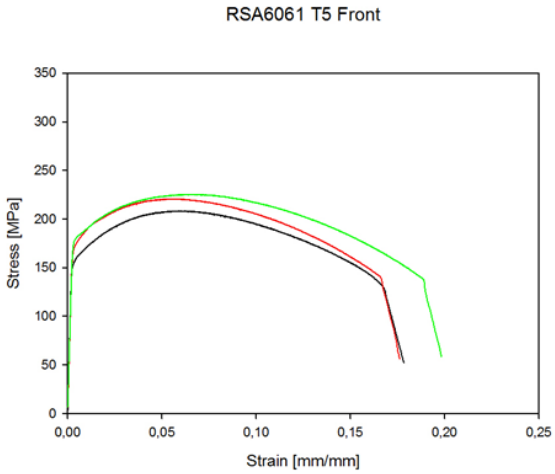

Figure 66: Tensile curves of RSA6061 T5 Front, with three parallels.

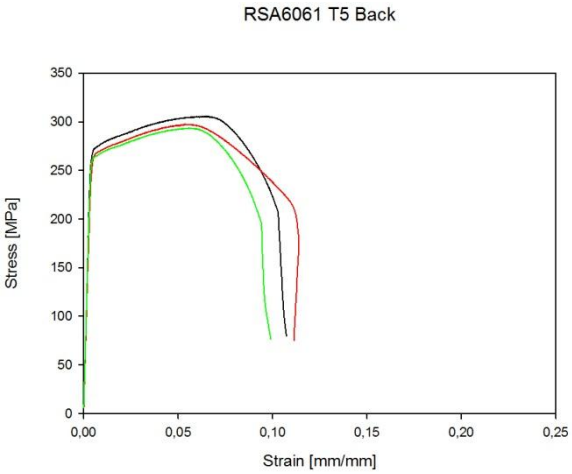

Figure 67: Tensile curves of RSA6061 T5 Back, with three parallels.

RSA6061 T6 520 (Figure 68) had the same problem as for the RSA6061T5 Back was the results are not valid after UTS, due to the extensometer knife fell into the necking. For the red graph, fracture was outside the extensometer. The yield strength was similar for all test parallels and there was a clear increase of strength from the T5 samples.

RSA6061 T6 580(Figure 69) tensile test samples had a lot of blisters and cracks due to the SSHT, and every sample fractured right after the yield point. The green graph show an increase of yield strength compared to SSHT at 520, while the two other graphs shows a decrease.

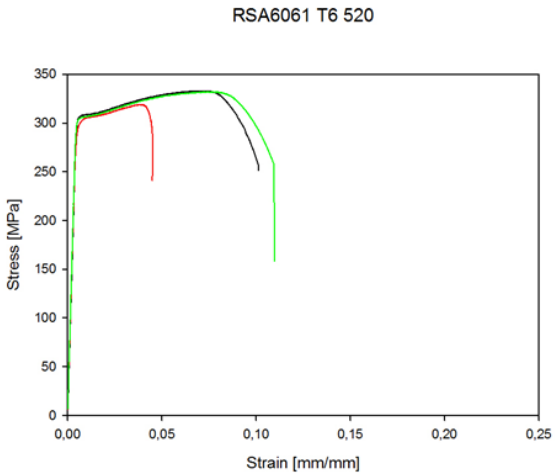

Figure 68: Tensile curves of RSA6061 T6 520, with three parallels.

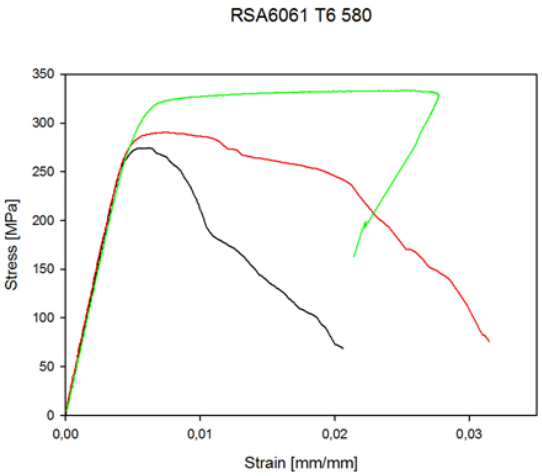

Figure 69: Tensile curves of RSA6061 T6 580, with three parallels. Please not the scale on x-axis.

4.2.5.4 Fractography

In Figure 70 to Figure 73 the fractography from one tensile specimen for each heat treatment, RSA6061 T5 Front, RSA6061 T5 Back, RSA6061 T6 520 and RSA6061 T6 580. Each figure shows the overview and some important details.

Figure 70 shows the fractography of RSA6061 T5 front. From the image in upper left corner, there can be observed “hills and valleys” in circles, this have been observed in screw extruded material before[6]. In the two lower fractographies there can be observed dimples from shear and tensile stress.

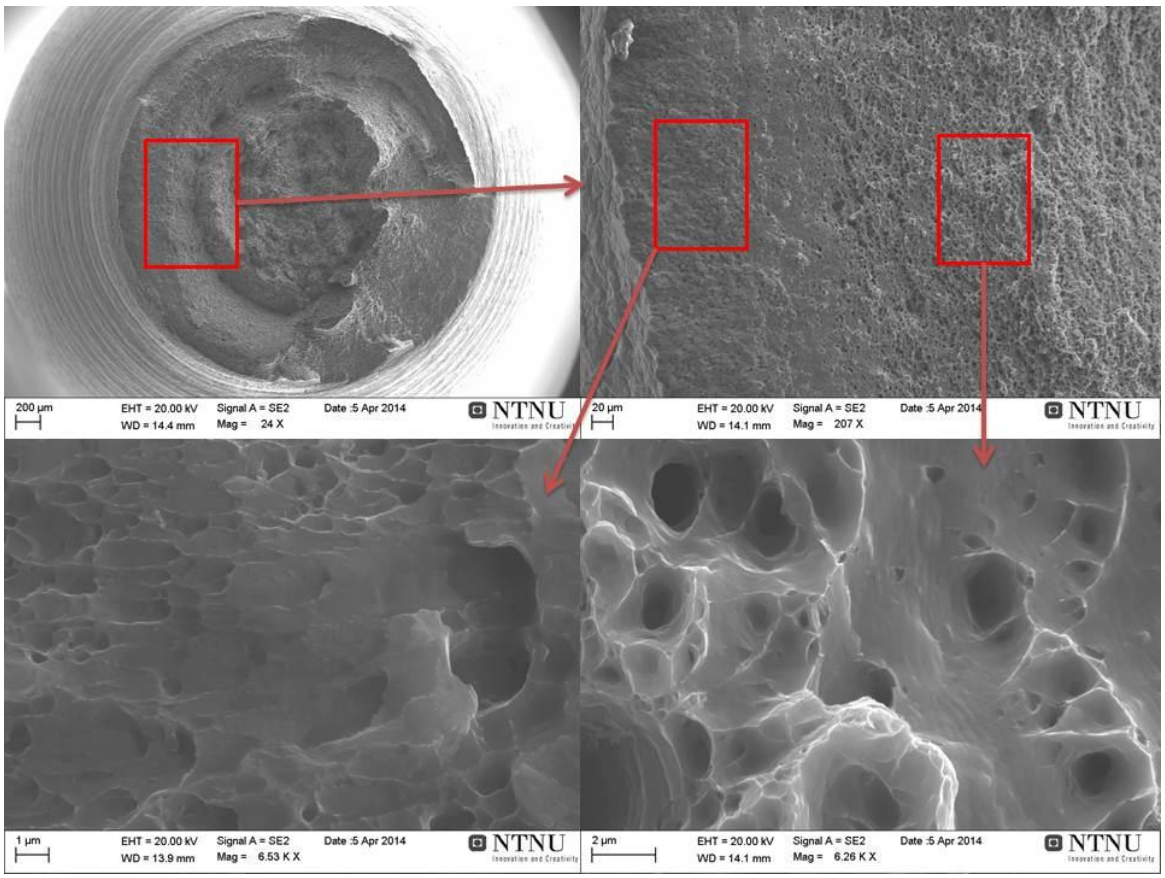

Figure 70: Fractography of RSA6061 T5 Front.

In Figure 71 the fractography of RSA6061 T5 Back is illustrated. The fracture has the same characteristics as the prior sample, with dimples in for of shear and tensile stress.

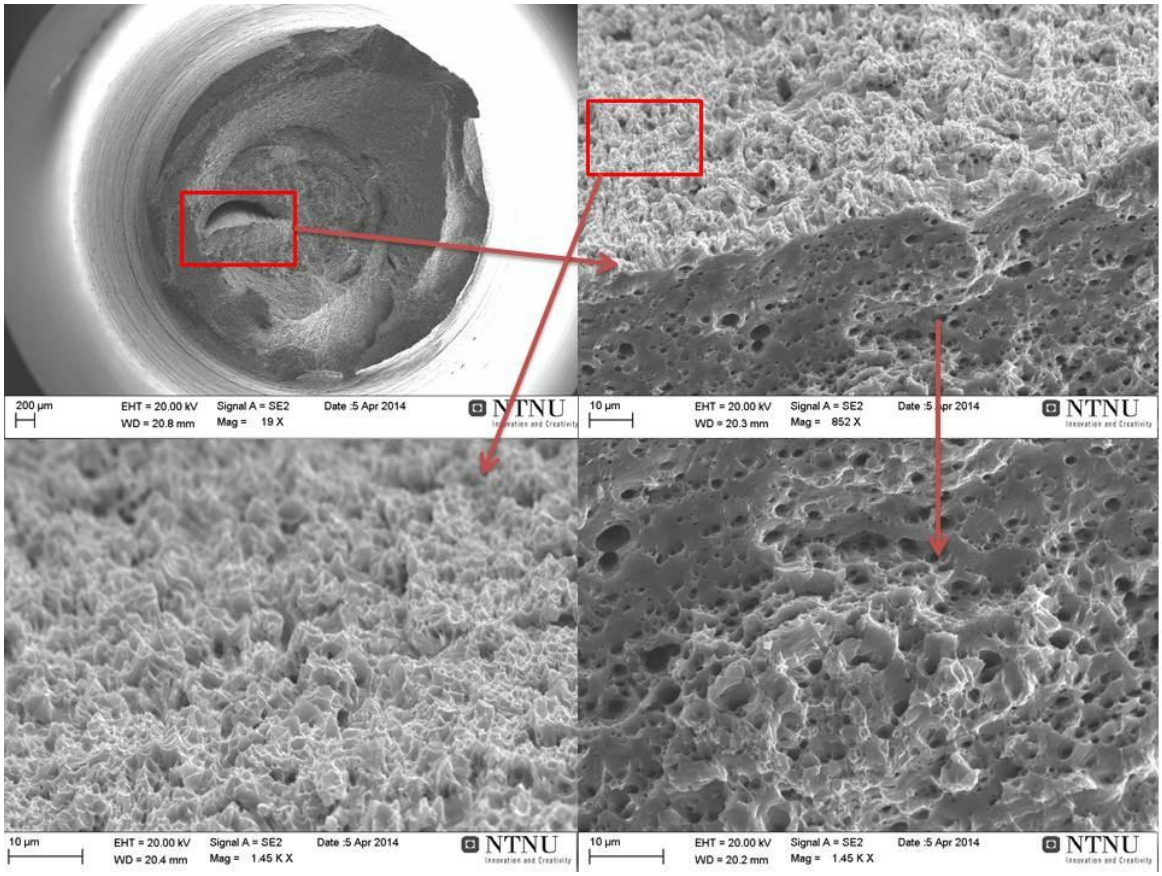

Figure 71: Fractography of RSA6061 T5 back.

The T6 sample with SSHT temperature of 520°C is shown in Figure 72. Here it is observed cracks, dimples and also some indication of brittle fracture near the cracks.

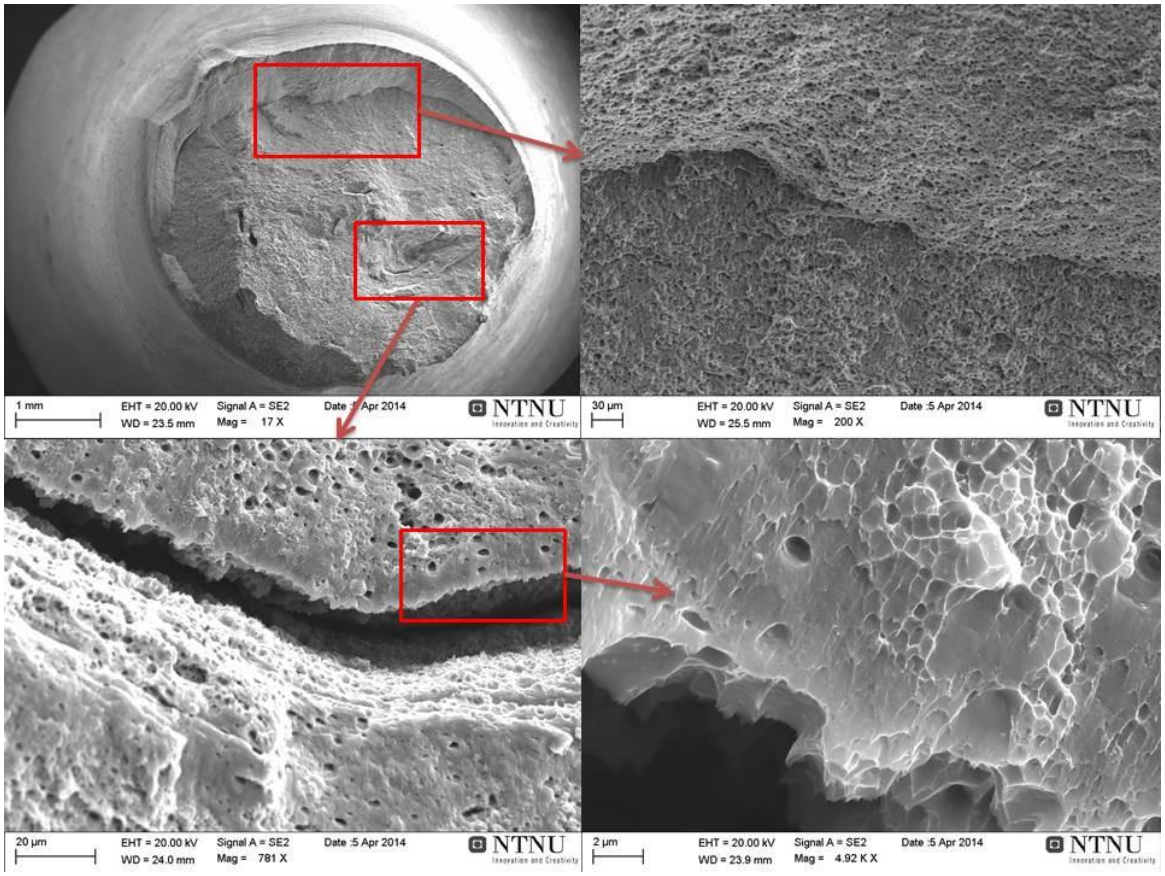

Figure 72: Fractography of RSA6061 T6, SSHT at 520°C.

The last fractography, Figure 73, is from the RSA6061 T6 580. The cracks are even bigger and numerous. There are observed shallow big dimples (~10µm in diameter) and smaller ones in between.

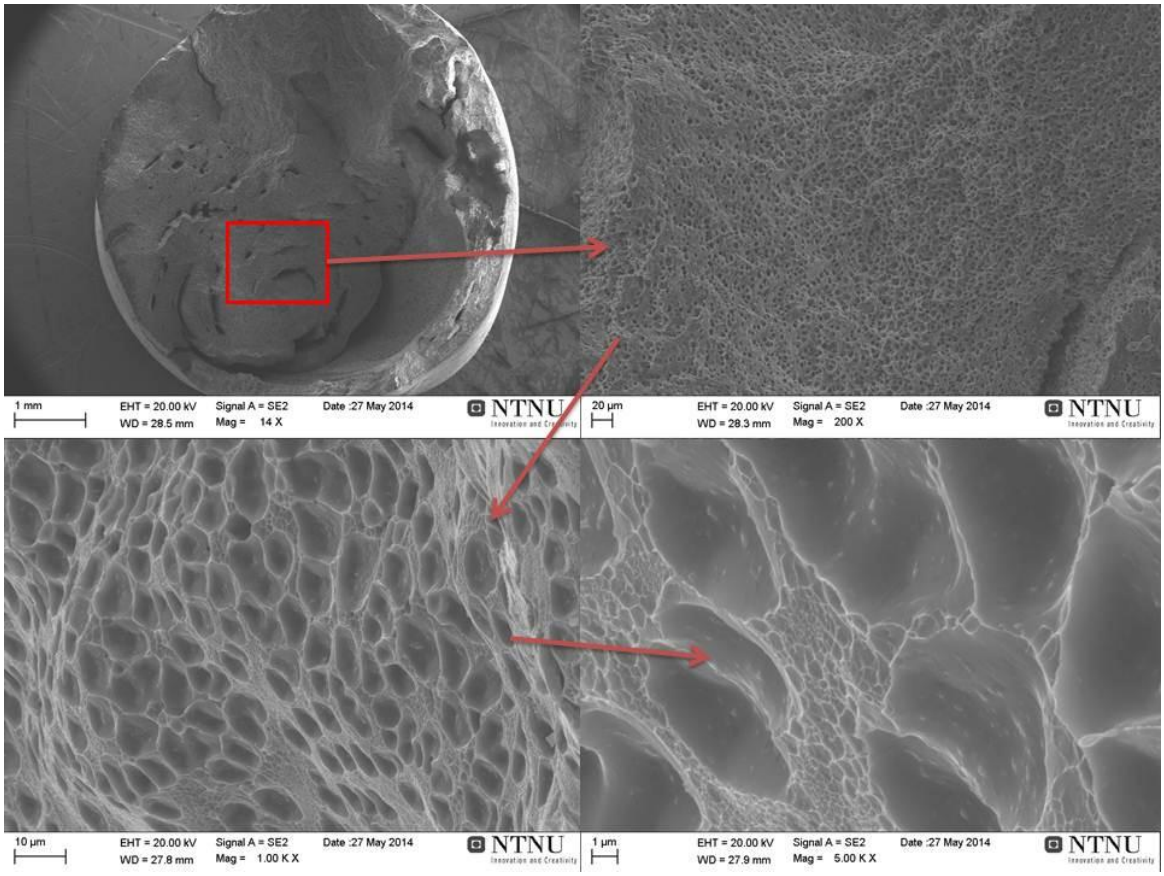

Figure 73: Fractography of RSA6061 T6, SSHT at 580°C.

4.3. EDS analysis of particles

This chapter sums up the EDS analysis and particles for previous sections. It is three main spectra that are observed, aluminium matrix (Figure 74), white particle (Figure 75) and black particle (Figure 76).

In Figure 74, intensity of aluminium is by far the highest, with a small top at magnesium and silicon. The intensity between 0 keV and magnesium is general noise. Note that the intensity for Cr, Mn and Fe is zero. The scan is from an area with no indication of particles.

Figure 75, illustrate a typical result of spot scan on a white particle. The intensity of aluminium is highest as in Figure 74, but it is a change in the intensity of Si, Cr, Mn and Fe. This indicates that there are more of the mentioned elements here, than in the matrix. Note that the exact composition cannot be analysed due to small particle (~0.1µm) compared to emission depth (~1.2µm).

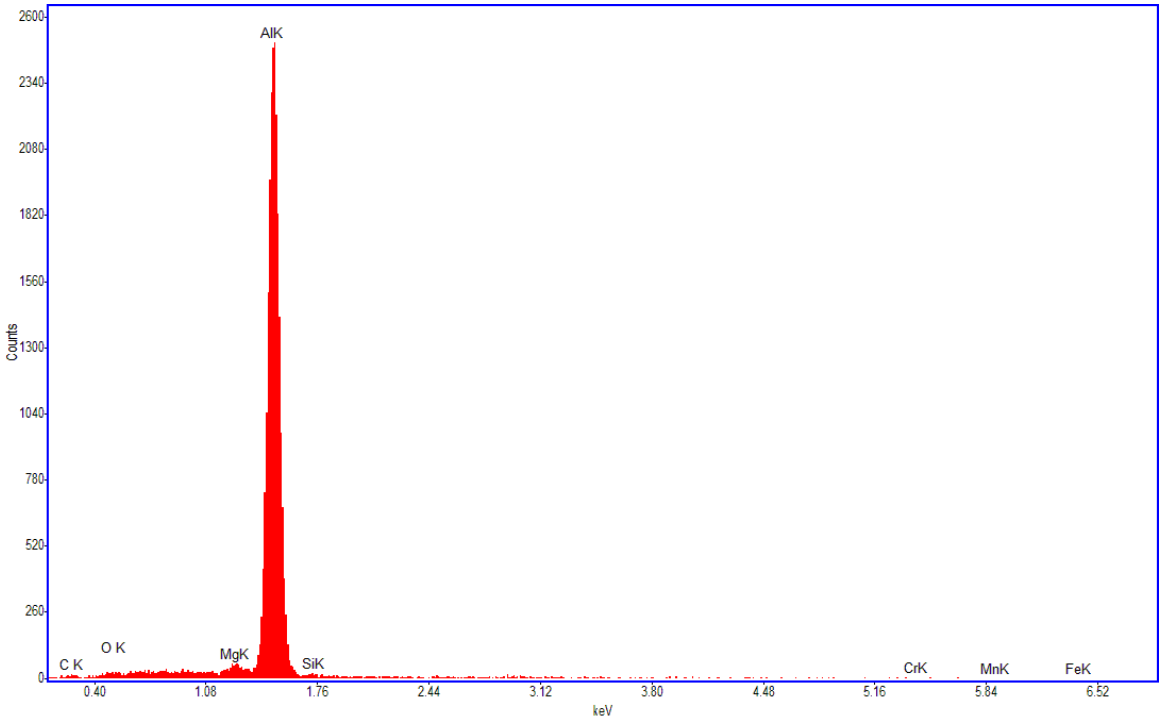

Figure 74: Example of energy dispersive spectra of the aluminium matrix, intensity versus characteristic spectra.

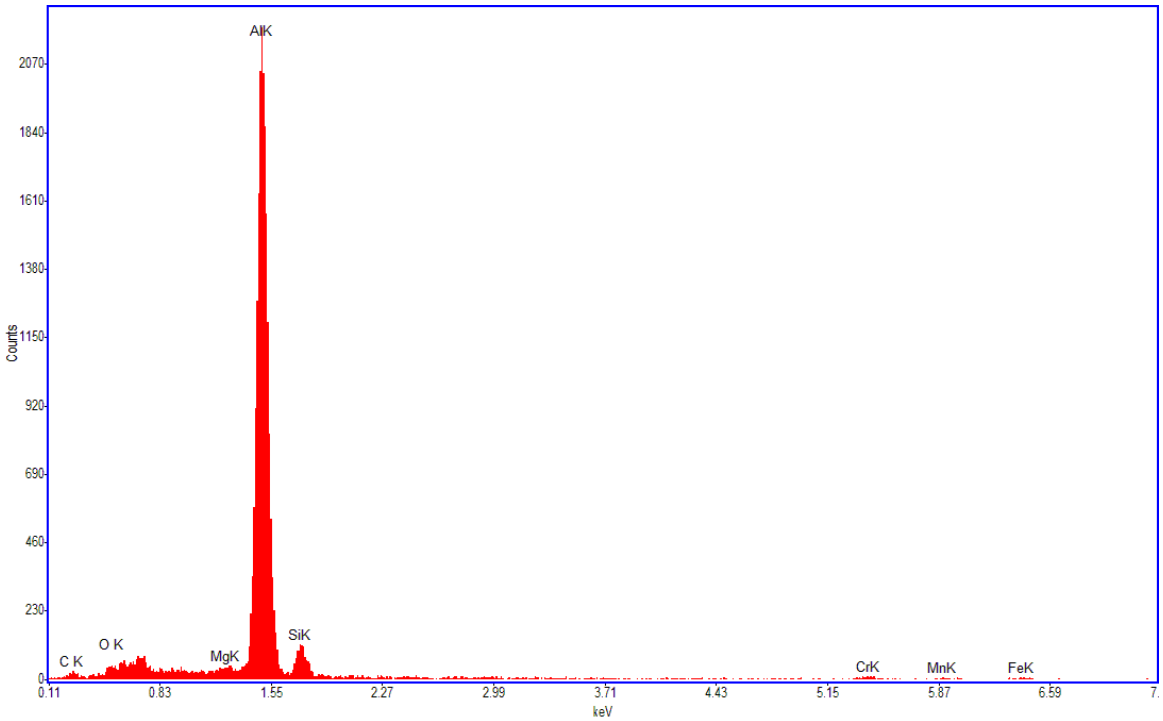

Figure 75: Example of energy dispersive spectra of white particles, intensity versus characteristic spectra.

The energy dispersive spectra of a black particle are illustrated in Figure 76. The intensity for aluminium is still highest, but Mg and Si have distinct tops. The ratio between Mg and Si is close to 2/1 which strongly indicates Mg_2Si particle. It is a small, but distinct intensity of oxygen, this can either come from oxidation of Mg or contaminations. The black particles (~1µm) are as the white particles (~0.1µm), smaller than the emission depth (~1.2µm) of the x-rays, which give high intensity of aluminium.

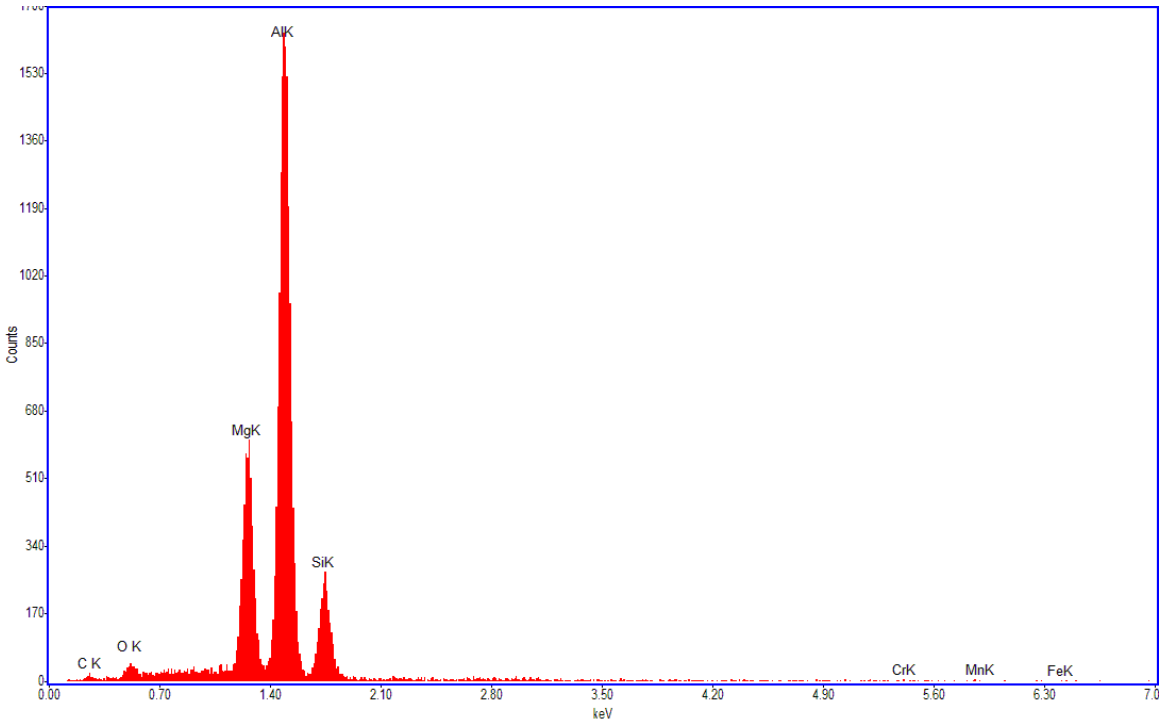

Figure 76: Example of energy dispersive spectra of black particle, intensity versus characteristic spectra.

5. Discussion

In this chapter, the results will be discussed in further detail. The effect of thermal history and heat treatments will be put in context. First, the RSP6061 granulates, the extrusion and EDS analysis will be discussed. Then, the effect of heat treatment on extruded profiles will be discussed.

5.1. EDS analysis of particles

The EDS analysis of particles is illustrated with three examples (Figure 74 to Figure 76) from this study, because the same alloy was used through the study and difficulty to quantify the elements in particles. As described in the theory and results, the emission depth is 1.2 - 1.3μm for reflected x-rays at 9keV.

With particles (white) that are a tenth of this, the aluminium will dominate the reflection intensity, i.e. there are only possible to determine which elements that is present. It is observed Si, Cr, Mn and Fe in the white particles, which indicates dispersoids. This seems likely due to the alloy content in Table 3. Due to the fact that the elements cannot be quantified, the exact content of the dispersoids will therefore not be discussed.

The analysis of the black particles shows a clear indication of Mg and Si, even though the aluminium intensity is still dominating. Mg and Si have distinct tops with a relatively high intensity, and Mg has two times the intensity of Si. Therefore black particles are assumed as Mg_2Si, the shape also indicates this.

5.2. As recived RSP6061 material

The rapid solidified (RS) material was extruded in the same thermal state as delivered from RSP-Technology[7]. The process parameters for production are not known, other than solidification by melt spinning and mechanically cutting/deformation from ribbons to granules. It is unknown when the material was produced and for how long the material has been stored, before the present investigations were performed. This can have an influence on the material properties, but due to lack of knowledge on the history of the material, it will not be discussed.

The solidification parameters are important to know in order to determine the solidification rate, grain size and amount of alloying elements in solid solution. In previous work[27] the hardness of the same granules was tested and a hardness of 100 to 110 Vickers hardness (1gf), was found through the thickness of the granules. This is a relative high hardness for solidified material. This indicates that the RS material should have the alloying elements in solid solution (solid solution strengthening), and as well as having a small grain size (grain boundary

strengthening). This indicates that the RSP6061 alloy in fact had been subjected to rapid cooling. The received material could also be work hardened from the mechanical cutting processing. This deformation can in fact be observed by looking at the material shown in Figure 16, i.e. because the granules are short and deformed.

By observation on the backscatter micrographs in section 4.1, particles with higher atom number than aluminium were observed. This can be small primary particles of Fe, Cu, Cr or Mn that were precipitated during solidification. Primary particles from DC-casting can be significantly bigger than the 100nm seen in Figure 31. The small size indicates that there are not "normal" solidification rates, but rapid solidification.

5.3. Extrusion and extruded profiles

As seen in Figure 17, the die temperature during the extrusion was quite steady around 530°C. A stable extrusion temperature should normally give homogenous properties throughout the extrusion length.

The present as-extruded profiles had no visible sign of defects (blisters or scratches) on the outside. The visible outer of the profiles and the observation during extrusion, indicate that the extrusion was successful. The estimated extrusion speed, displayed in Table 9, showed an extrusion speed of approximately 1cm/s. Because of the measurement method with a stop watch, the exact value is not relevant, but the magnitude of the extrusion speed is illustrated. This is used to estimate the time the different sections of the profile (front and back), is chilled in air before quenching in water. By this calculation the RSA6061F Front was up to 50 seconds in air before quenching. The profiles were cut in ca, 40cm long pieces and the cutting was done 10cm from the die opening. This gives a total length of the extruded profile of 50cm, and with an extrusion speed of 1cm/s this gives an air chill time of ~50 seconds before quenching. Applying the same calculations approach, RSA6061F Back will have an air chill time of 10 second before quenching. This rough estimate show that one cannot treat the front and back as being in the same state, due to the dwell-time difference at high temperature and the different cooling rates for the Front and the Back. This is clearly reflected in the artificial aging curves (Figure 50) and tensile test (Figure 66 and Figure 67) of the T5 samples.

The hardness testing of the cross- and longitudinal-section of the RSA6061F (Figure 33) showed no clear tendency of strength difference through the thickness of the sample. The hardness differs maximum 4HV1 from the hardest to the weakest and then with a varying standard deviation. Accordingly no obvious structural difference through the thickness of could be observed, which suggests a homogeneous microstructure.

5.3.1. EDS analysis for extruded profiles

In the backscatter micrographs there were two important findings. First the black round particles and second the white smaller particles. The black particles were

evenly distributed in the samples, but having a varying size. From the shape, spectrograph analysis and the thermal history it is believed that these latter particles are Mg_2Si. The shape is not perfectly circular, but they have sharp corners and straight edges, which indicates Mg_2Si. The growth mechanism of Mg_2Si described in the literature, manifests that this precipitate grows in the [100] direction followed by the [111] direction, i.e. in to a polygon. The spectrographs also indicate that these particles are Mg_2Si, because the intensity of Mg and Si is significant at the particle compared to the surrounding matrix. However, the intensity of aluminium is generally higher in all the spot scans, and this intensity should then come from the surrounding matrix of aluminium. Utilizing Figure 14 and an acceleration voltage of 9kV, this will give an emission depth between 1.2μm and 1.3μm. When the particle is smaller than this, the surrounding matrix will be analysed as well. Because of many small particles it is not possible to give an exact composition of any of the particles in this study, i.e. all measured particles were less than 1μm in diameter.

5.4. The heat treatments effect on strength

The two main results that sums up this study, are the tensile tests and the age hardening curves of the different thermal states. Everything done on the material after extrusion will affect the strength of the material. In this part of the discussion, each thermal state will be discussed in relation to microstructure, particle distributions and heat treatments. Each of them will be related to the strength and compared.

5.4.1. As extruded and artificially aged samples (T5)

The two different T5 states in this study were RSA6061T5 Front and RSA6061T5 Back. The tensile tests and the age hardening curve (Figure 50) of the Front showed a material that has low to no effect of age hardening. The strength of the front material is relatively low for a 6061 alloy in the age hardened state, and the age hardening curve did not have the typical shape. The effect of age hardening to maximum strength is only about 10HV and there is no typical overaged state after this. The material gets stronger after five days, instead of weaker. This probably means that the precipitation kinetics are slower than usual, i.e. probably due to a low driving force originating from a small chemical potential for precipitation.

However, the RSA6061T5 Back showed a typical age hardening. The age hardening gives an increase in strength of about 60% at the peak hardness, and show an overaged state were the hardness is lowered. This indicates that the age hardening was successful and that a significant amount of the alloying elements were in solid solution.

To determine the reason for difference for the front versus the back material, the microstructure and particle analysis of the material also had to be compared.

The micrographs of RSA6061F (as extruded, front and back) samples, show a homogenous microstructure without cracks or recrystallized zones. There is no indication of abnormal grain growth at the surface during the extrusion, neither any formation nor growth of cracks. The average grain size is measured to approximately 7μm, and seems to be homogenous through the thickness of the profiles. The fairly bigger grain size in RSA6061F Front might be described by grain growth during the air chill (after extrusion), where the profiles have a longer time at elevated temperature. The difference in average grain size between front and back is so small (0.5μm) that it is difficult to conclude anything, e.g. due to the unknown cooling rate in air.

When looking at the backscatter micrographs (Figure 36 and Figure 37), there are no clear difference in dispersoids and Mg_2Si for front and back. The size and distribution of the particles are almost the same. The measured amount of Mg_2Si does neither give a clear answer. There are measured more small Mg_2Si in the Front and more big Mg_2Si in the Back. From these data a conclusion cannot be made whether there are more Mg_2Si that are precipitated in the front than in the back of the cut profile. Even though this should be likely, due to the longer air chill time at the front. However it is possible that the Mg and Si have precipitated as β', but these are not visible at this magnification in the SEM. The β' can precipitate on dispersoids and therefor there is less available Mg and Si in solid solution for age hardening[14]. The RSA6061F Back should, by the obtained effect of age hardening, have more alloying elements in solid solution. This would be a clear case if there was a measurable difference of Mg_2Si in the Front and the Back. However, a comparison of the conductivity could add valuable information in this regard.

The dispersoid analysis (Figure 38) shows that there are more dispersoids in the front than in the back, especially of the smallest ones. This may have happened during extrusion and that the alloying elements as Mn, Fe or Cr that were in solid solution before extrusion, may have precipitated during the air chill. However it is important to note that dispersoids were even observed in the rapid solidified granules, i.e. they should be existing through the whole thermal history of this material. Therefor the difference in dispersoids seems even more unlikely. It is also possible that there is an inconsistency in the measuring procedure due to the human error in the threshold and contrast manipulation of the micrographs before counting.

With the measured amount of Mg_2Si and dispersoids, most likely that precipitated β' on dispersoids are the main reason for the strength difference between back and front.

Moreover, the RSA6061F Back results indicate if the quenching procedure is more efficient than in this study, it should be possible to get a higher strength after the T5

heat treatment. Due to this assumption, PhD candidate K. Skorpen has designed and ordered a new quenching system for the screw extruder.

5.4.2. SSHT and age hardened samples

5.4.2.1 The effect of SSHT

The T6 samples in this study had four different SSHT temperatures; 520°C, 540°C, 560°C and 580°C. The strength of these different states from the artificial aging curves is almost identical. The maximum hardness is 112HV1 for all. The tensile tests of RSA6061 T6 520 and 580 indicate an increase of strength compared to RSA6061 T5 Back. These tensile specimens had several flaws that gave a big impact on the result, which need to be taken in account in the following. The constant hardness and tensile strength increase will be discussed as to microstructure from SSHT and age hardening.

The effect of the SSHT was investigated with hardness measurements (Figure 39) and electric conductivity (Figure 40). Theoretically, the peak-aged hardness is higher when all alloying elements are in solid solution than when equilibrium phases and particles are precipitated before age hardening. A significant amount of Mg2Si indicates a small amount of alloying elements in solid solution. This leads to a low hardness. From Figure 39, where the hardness is illustrated, it can be seen that the hardness is highest for a SSHT temperature of 520°C. From the result, there should be more alloying element in solid solution with the lowest SSHT temperature. This is not in correlation with the phase diagram and the composition of this alloy, because the SSHT temperature needed to get maximum alloying elements in solid solution is close to the eutectic temperature of 595°C. It is important to note that the hardness difference is small in regard to the various SSHT temperature, and the standard deviations are relatively large. The electric conductivity shows a different pattern, i.e. the conductivity is decreasing with increasing SSHT temperature. Basic theory on conductivity states that the conductivity is decreasing with increasing amount of alloying elements in solid solution. This seems to fit here. The measured conductivity is about 21% lower at SSHT temperature of 580°C than 520°C, which is significant. It is important to note that the standard deviation is varying for the different conditions, but the trend convincing. The overall trend indicates that a right SSHT temperature, introduces more elements in solid solution and this impacts that the peak-aged tensile test results accordingly.

The trend of more alloying elements in solid solution at higher SSHT temperature is also seen in the particle analysis. The number of Mg_2Si is decreasing drastically from a SSHT at 540°C to 560°C and even more at 580°C. From Figure 49, there seems to be a lot of small Mg_2Si particles in the size range 0.2-0.3µm, but compared to the backscatter micrographs this do not correspond. Here the challenge with the particle count is clear, and therefore the smallest particles that are counted can be discussible. The effect of less Mg_2Si is more Mg and Si in solid solution, which can

precipitated as β´´. Therefore, the potential for age hardening are increasing with increasing SSHT temperature, i.e. in the accordance to basic theory.

Moreover, it seems to be small changes in the dispersoid distribution when performing the SSHT and artificial aging compared to the "as extruded" profiles. However, the trend of decreasing amount of particles with increasing particle size is still valid. There is not a significant difference between the different SSHT temperatures, but there is a decreasing amount of dispersoids with increasing SSHT temperatures. This dependency to the SSHT temperature is not significant so this can not be concluded. The fact that the driving force for diffusion is higher for higher temperatures supports the results, but the time span is only ten minutes. Therefor it is not easy to claim whether the dispersoids are dissolving at high temperature there is an over-running inaccuracy in the measurements.

The optical micrographs illustrate another important effect on the microstructure, namely recrystallization. This is documented for RSA6061W 560 and 580, but during the study it is also observed at 540°C. The recrystallized zone widths are not constant along the profile, this can be seen from the uneven thickness of recrystallized zone. Earlier studies by Bilsbak[1] do confirm the same. Recrystallization is not observed in the centre or around cracks, so it seems that the high friction stress at the profile surface is an important factor for the driving force for recrystallization. This is logical and follows the theory on extrusion, i.e. that the friction stress is higher on the surface, than in the centre. It has been observed previously that the material in the centre of the profile is not steady, but is moving from one side, to the other [4-6]. This could probably effect the friction stress on the surface, and therefor the amount of deformation on the material. The highest deformed zones could favour abnormal grain growth. It should here be added that the recrystallized zone can have a negative effect on strength due to less grain boundary strengthening.

The grain size can have been affected by the SSHT temperature. A small increase of grain size with increasing SSHT temperature was in fact measured. The driving force for grain growth is highly temperature dependent and an increase of temperature can give grain growth[23]. The effect of grain size on the strength of the material is important, and the presence of larger grains will affect the strength in a negative manner.

5.4.2.2 The effect of age hardening after SSHT

After artificial aging the profiles got a further development in the microstructure. for the amount of Mg_2Si and dispersoids, only minor changes occurred. The RSA6061 T6 520 and 540 still contained coarse Mg_2Si, while the 560 and 580 had very little to none. These results are as expected, because the temperature that Mg_2Si can dissolve is much higher. At 185°C β`` will disperse, while nothing happens to the coarse $Mg_2Si$. The β`` is not visible at the utilized magnification and can therefore not

be observed (needs transmission electron microscopy). The dispersoids are still present without any big difference from before age hardening. Due to constant amount of dispersoids, the material will not change the potential for strength introduced by a more refined grain structure.

When analysing the result of the optical micrographs (Figure 54 to Figure 57) a lot more have happened. It is measured a slight increase in grain size, at 520°C and 540°C, but this is marginal (about 4%), while the 560°C and 580°C had 12% and 13% increase in grain size respectively. This is a large difference, but the standard deviation is also significant, 0.71µm or a difference of ±9% for 580°C. If this is the case, the larger grain size will have a negative effect on strength due to less grain boundary strengthening.

The recrystallized zones seen in the profiles after SSHT are also observed in the optical micrographs. In the T6 condiction, the recrystallized zones at the surface are abnormally big, with a maximum of 1300µm width in the 580°C sample. It is still no recrystallized zone in 520°C and 540°C, so these do not recrystallize during age hardening. This seems naturally since the recrystallization temperature is normally higher for dispersoid-containing alloys [28, 29]. The dispersoids also give a pinning effect on grain growth and will therefor retard the growth of abnormal big grains. The fact that abnormal grain growth happens at higher temperatures, makes it unlikely that the samples have entered abnormal grain growth during age hardening. Here the material flow instability from the screw, which can lead to different shear stress through the thickness of the sample, can explain the different thicknesses of the recrystallized layer (due to higher friction stress at the surface). Secondary recrystallization at the surfaces will probably have a negative effect on strength, due to less grain boundaries and boundary strengthening.

The last possible effect that can explain a constant hardness in the artificial aging curves is recovery. The results show that by increasing the heat input (higher SSHT temperature), the hardness will remain the same. Even though the potential for age hardening increases with increasing SSHT temperature. Therefor it seems that there have been a recovery effect on the material, which will lower the YS and UTS. The recovery therefore seems to compensate the potential for strength contribution from more alloying element in solid solution with increasing SSHT temperatures.

5.4.2.3 Heat treatment effect on cracks

It is seen through the heat treatment steps, SSHT and age hardening, that a lot of cracks have been developed in the material. This has clearly a correlation with the temperature. With increasing heat input, there is an increase in size and numbers of cracks. These should not have a direct influence on the strength of the material (UTS) and ductility, since final failure appears to early while the material is in the work hardening stage and facture occurs almost instantly. However, the cracks should not impact the hardness as long as the indications are taken outside the

cracks. The cracks can either come from dirt on the RSP6061 granules, e.g. trapped inside the material, or hydrogen in the aluminium oxide. It is not likely that the main reason is dirt, due to the washing and drying (section 3.3) and therefore a relatively clean base material. The more likely answer is hydrogen development from the high amount of oxides from rapid solidification. The oxide/aluminium ratio from melt spinning compared DC-casting is high due to big surface area against air. When these oxides get a big enough heat input, the barrier for hydrogen development is breached and trapped hydrogen gas will force crack formation in the material.

5.4.2.4 Fractography

The fractographies from section 4.2.5.4 show that all samples had a fraction of ductile behaviour. It seems that there are two main ductile fracture mechanisms, tensile and shear. Tensile, obviously from the tensile force, while shear is introduced from the "hills and valleys" developed due to defects in the material, plus cracks developed during SSHT.

6. Conclusion

In this study there screw extrusion has been utilized on rapid solidified aluminium and profiles having a diameter of 10mm were produced. The profiles were analysed "as extruded", after solid solution heat treatment and age hardening to T5 and T6. Optical microscopy, SEM, hardness measurements and tensile tests were used to characterize the materials.

- The RSP6061 granulates have a relatively high hardness and containing dispersoids with a content of Fe, Cr and/or Mn.
- Screw extrusion of rapid solidified material was successful, with a relatively steady die temperature of 530°C. The extrusion speed was approximately 1cm/s and there were no visible defects on the extruded profile surfaces.
- The mechanical properties of the "as extruded" profile are close to homogenous, and the profiles contained no internal cracks nor recrystallized layer.
- The need for controlled cooling of the extruded profile is essential to get a homogenous microstructure along the length of the profiles. The cooling rate is also significant regarding artificial aging.
- SSHT give a positive effect for the hardenability compared to "as extruded" profiles. The maximum strength difference is about 10%, comparing the "as extruded" and SSHT + aged conditions.
- It is little or no effect on strength for the different SSHT temperatures. The hardness at peak is 112HV1 for all SSHT temperatures. The effect of coarse Mg_2Si is documented, and an increasing SSHT temperature decreases the amount of coarse Mg_2Si. This indicates a potential for strength increase at higher SSHT temperatures. However, this could never be documented by tensile test since the embedded cracks caused early failure while the material still was in the rapid work hardening phase.
- The profiles get abnormal grain growth at the surface during SSHT temperature of 560°C and 580°C.
- Cracks and pores are developing during SSHT, this is documented for all SSHT temperatures. Observations indicate that the amount of cracks increase with increasing SSHT temperature.

1. Bilsbak, A., *Microstructure and mechanical properties of screw extruded aluminium : Characterization of screw extruded aluminium with respect to different cleaning techniques for the feedstock.*MSc thesis, IMT, NTNU 2012.
2. Mauland, E., *Utherdbare bimetall materialer fremstilt ved skrueekstrudering: AA 6060/ren magnesium*. 2013, Institutt for materialteknologi, NTNU.
3. Pedersen, B.D., *Preliminary Investigations on the Manufacture of Al-AZ31 Bimetallic Composites by the Screw Extrusion Process*. 2013, Institutt for materialteknologi, NTNU.
4. Widerøe, F., *Material Flow in Screw Extrusion of Aluminium*. PhD thesis. 2012: NTNU.
5. Widerøe, F. and T. Welo, *Using contrast material techniques to determine metal flow in screw extrusion of aluminium.* Journal of Materials Processing Technology, 2013. **213**(7): p. 1007-1018.
6. Skorpen, K.G., *Characterization of extruded Aluminium*, IMT, NTNU. 2011, NTNU.
7. RSP-Technology. 2013; Available from: http://www.rsp-technology.com/.
8. Solberg, J.K., *Teknologiske metaller og legeringer*. 2010, Trondheim: NTNU.
9. Belov, N.A., D.G. Eskin, and A.A. Aksenov, *Multicomponent phase diagrams: applications for commercial aluminum alloys*. 2005, Amsterdam: Elsevier.
10. Li, C., et al., *Morphological evolution and growth mechanism of primary Mg2Si phase in Al–Mg2Si alloys.* Acta Materialia, 2011. **59**(3): p. 1058-1067.
11. Reiso, O. 2014. personal communication.
12. Werenskiold J.C , A.L., Roven H.J, Ryum N, Reiso O., *Screw extruder for continuous extrusion of materials with high viscosity*. 2010. patent
13. Hatch, J.E., A. Association, and A.S.f. Metals, *Aluminum: Properties and Physical Metallurgy*. 1984: American Society for Metals.
14. Reiso, O., *Extrusion of AlMgSi alloys.* Mater. Forum, 2004. **28**: p. 32-46.
15. Askeland, D.R., et al., *The science and engineering of materials*. 2011, Stamford, Conn.: Cengage Learning. XXIII, 920 s.
16. Andersen, S.J., et al., *The structural relation between precipitates in Al–Mg–Si alloys, the Al-matrix and diamond silicon, with emphasis on the trigonal phase U1-MgAl2Si2*. Materials Science and Engineering: A, 2007. **444**(1–2): p. 157-169.
17. Polmear, I.J., *Light alloys: from traditional alloys to nanocrystals*. 2006, Amsterdam: Elsevier/Butterworth-Heinemann. 1 online resource (xiv, 421 s.).
18. Dons, A.L. and O. Lohne, *Quench Sensitivity of Almgsi-Alloys Containing Mn or Cr*. MRS Online Proceedings Library, 1983. **21**:
19. Humphreys, F.J., *A unified theory of recovery, recrystallization and grain growth, based on the stability and growth of cellular microstructures—I. The basic model.* Acta Materialia, 1997. **45**(10): p. 4231-4240.
20. Humphreys, F.J. and M. Hatherly, *Recrystallization and related annealing phenomena*. 2004, Amsterdam: Elsevier. 628 s.
21. Rollett, A., F.J. Humphreys, and G.S. Rohrer, *Recrystallization and Related Annealing Phenomena*. 2004: Elsevier Science.
22. Porter, D.A., K.E. Easterling, and M.Y. Sherif, *Phase Transformations in Metals and Alloys*. 2009: Taylor & Francis Group.
23. Dieter, G.E. and D.J. Bacon, *Mechanical Metallurgy*. 1988: MCGRAW-HILL Higher Education.
24. Hjelen, J., *Scanning elktron-mikroskopi*. 1989.
25. *RSP-Technology* 2013; Available from: http://www.rsp-technology.com/.

26. *RSP-Technology*. 2013; Available from: http://www.rsp-technology.com/RSP%20Technology%20-%20Alloy%20Overview.pdf.
27. Stedje, T., et al., *Rapid Solidified Alumnium Alloys*. 2013, NTNU.
28. Li, X., M.E. Kassner, and S.C. Bergsma, *Recrystallization behavior of rolled ingots of 6061 and 6069 aluminum alloys.* Journal of Materials Engineering and Performance, 2000. **9**(4): p. 416-423.
29. Kashihara, K. and H. Inagaki, *Effect of Precipitation on Development of Recrystallization Texture in a 6061 Aluminum Alloy*. MATERIALS TRANSACTIONS, 2009. **50**(3): p. 528-536.

A. Grain size macro script

```
Sub enpixler()

siste = Range("B3").End(xlDown).Row
Korn = 0

For n = 2 To siste
   If Range("B" & n) <> Range("B" & (n - 1)) Then
      If (Range("B" & n) <> Range("B" & (n + 1)))
Then
      Else
         Korn = Korn + 1
      End If
   End If
Next

Range("B1") = Korn
```